

Accepted Manuscript

A Mathematical Investigation of the Turkevich Organizer Theory in the Citrate Method for the Synthesis of Gold Nanoparticles

Emmanuel Agunloye, Asterios Gavriilidis, Luca Mazzei

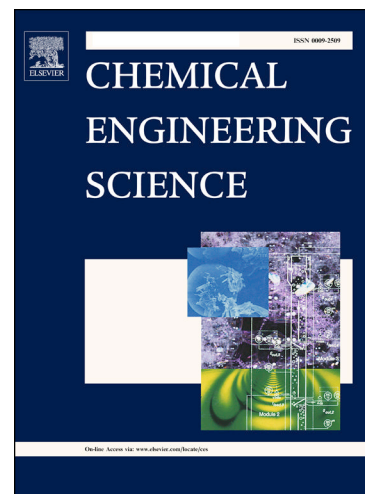
PII: S0009-2509(17)30474-8
DOI: <http://dx.doi.org/10.1016/j.ces.2017.07.032>
Reference: CES 13727

To appear in: *Chemical Engineering Science*

Received Date: 17 March 2017
Revised Date: 26 May 2017
Accepted Date: 16 July 2017

Please cite this article as: E. Agunloye, A. Gavriilidis, L. Mazzei, A Mathematical Investigation of the Turkevich Organizer Theory in the Citrate Method for the Synthesis of Gold Nanoparticles, *Chemical Engineering Science* (2017), doi: <http://dx.doi.org/10.1016/j.ces.2017.07.032>

This is a PDF file of an unedited manuscript that has been accepted for publication. As a service to our customers we are providing this early version of the manuscript. The manuscript will undergo copyediting, typesetting, and review of the resulting proof before it is published in its final form. Please note that during the production process errors may be discovered which could affect the content, and all legal disclaimers that apply to the journal pertain.



A Mathematical Investigation of the Turkevich Organizer Theory in the Citrate Method for the Synthesis of Gold Nanoparticles

Emmanuel Agunloye, Asterios Gavriilidis, Luca Mazzei*

Department of Chemical Engineering, University College London,
Torrington Place, WC1E 7JE, UK

*corresponding author: Luca Mazzei; email address: l.mazzei@ucl.ac.uk

Abstract

Gold nanoparticles are commonly manufactured by the citrate reduction method, a synthesis method pioneered by Turkevich et al. (1951). Based on their experimental evidence, Turkevich et al. (1951) advanced the organizer theory, a nucleation-growth synthesis mechanism. Subsequently, Kumar et al. (2007) developed a mathematical model for the description of the synthesis, basing it on such a theory. However, this model has not been thoroughly tested. Recently, contrary to the evidence provided by Turkevich et al. (1951), other mechanistic descriptions of the synthesis, which emphasize the role of the pH of the solution, have been advanced in the literature. In this paper, we investigated the model of Kumar et al. (2007) for different conditions of pH, temperature and initial reactant concentrations. To solve the model, we used the numerical code Parsival, which is used for solving population balance equations. We tested the model for different synthesis conditions studied experimentally by various researchers, for which results are available in the literature. The model poorly predicted the experimental data because the Turkevich organizer theory does not account for the acid-base properties of chloroauric acid and sodium citrate. A new model, with a more accurate mechanistic description of the synthesis and of the chemistry involved, is therefore required.

Keywords

Gold nanoparticles; Citrate reduction method; Turkevich organizer theory; Population balance modelling; Parsival.

1 Introduction

Research in nanotechnology is increasing and is prioritized in developed countries such as the United States, the United Kingdom and Japan. This technology exploits the unique properties of nanoparticles. These are particles ranging from 1 to 200 nm. Depending on the type of material, nanoparticles can be broadly divided into four classes: metallic, semiconductor, magnetic and others (Liveri, 2006). In this work, we focus on metal and, in particular, gold nanoparticles.

Gold nanoparticles (GNPs) are important in many applications of nanotechnology, because they are inert and optically active. In biomedicine, for example, especially in the treatment of cancer, GNPs are highly effective. Different biomedical applications, however, require GNPs of different sizes. For instance, for tumor therapy in humans the optimal particle size is 50 nm, whilst for tumor diagnosis it is 20 nm (Dreifuss et al., 2015). Performance and properties of GNPs depend strongly on particle size and shape. The citrate method is the most common method for producing spherical gold nanoparticles. Using it, researchers have synthesized GNPs of sizes in the range 9 to 150 nm, which are potentially useful in several applications. However, the GNPs produced are usually polydisperse and often irreproducible.

A model of the synthesis would help to select the conditions in which to produce the particles and to design the reactor in which the synthesis is to be conducted; this would enable to control the process better and render the GNPs more reproducible. However, before developing a model, one needs to understand, or at least have a theory to describe, the mechanisms governing the synthesis. A model built on this mechanistic description, in turn, would permit testing the latter and thereby acquiring a better grasp of the synthesis mechanisms. In 1951, Turkevich and co-workers pioneered the citrate reduction method, using electron microscopy to investigate how the GNPs evolve during the synthesis. Their findings made them advance the popular “Turkevich organizer theory”. According to this theory, sodium citrate reduces chloroauric acid to aurous ions and concurrently oxidizes to dicarboxy acetone. Subsequently, by bringing together (that is, by “organizing”) a sufficient number of aurous ions, dicarboxy acetone causes gold nuclei to form. Concurrently, it also decomposes into acetone, eventually arresting the nucleation process. Once this has happened, the remaining aurous ions make the nuclei grow. This justifies why this theory is also referred to as “nucleation-growth” theory.

Subsequently, Frens (1973) studied this synthesis and demonstrated that different sizes of GNPs can be obtained by changing the concentration of sodium citrate while keeping the concentration of chloroauric acid at about 0.3 mol/m^3 . This technique was slightly modified by Freund and Spiro (1985) to produce GNPs used for testing size-dependent catalytic properties of the particles. Abid (2003) used the synthesis to form different sizes of GNPs intended for laser and optical properties. However, unlike Frens (1973), Abid (2003) varied the concentration of both chloroauric acid and sodium citrate. Chow and Zukoski (1994) also explored the synthesis, this time by varying the concentration of chloroauric acid while keeping that of sodium citrate at 1.6 mol/m^3 . Unexpectedly, they observed that the particles aggregated. In 2007, Kumar and co-workers rationalized these experimental data, developing a model for

the synthesis based on the mechanism proposed by Turkevich et al. (1951). The model predictions fitted reasonably well the data of the latter and of many of the other researchers mentioned above [for details, we refer to Kumar et al. (2007)].

Recently, nevertheless, with the advent of new techniques such as the small angle X-ray scattering and X-ray absorption near edge spectroscopy, many authors have investigated the synthesis, stressing the importance of the role played by the pH of the reaction solution. Ji et al. (2007), for example, reduced the polydispersity of the particles by increasing the pH of the solution. They observed that the nucleation-growth mechanism occurs only when the pH is above 6.5. Below, they observed that GNPs evolve by nucleation, aggregation and intraparticle ripening. Similarly, when performing the synthesis at 75 °C, for initial pH values of the precursor between 3 and 5, Wuithschick et al. (2015) reported that nuclei aggregate until forming particles of stable size, which they called seeds. Thereafter, these grow into the final GNPs. This description is referred to as “seed-mediated” mechanism. Moreover, in a recent publication, Kettemann et al. (2016) discussed the importance of the speciation of the precursor and reducing agent at different pH. This aspect of the synthesis is not accounted for in the theory of Turkevich et al. (1951) and, consequently, in the model developed by Kumar et al. (2007).

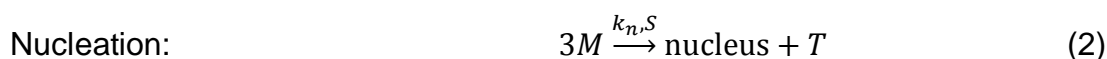
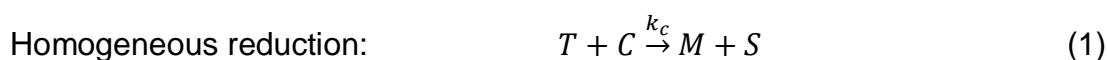
In light of this evidence, in this paper we intend to test the Turkevich organizer theory by investigating the model of Kumar et al. (2007). We first review the model and then we test it under new conditions, by comparing its predictions to experimental data available in the literature. In testing the model, we consider factors such as the initial concentrations of the precursor and reducing agent, the initial and final pH of the reaction solution, and the temperature of the latter.

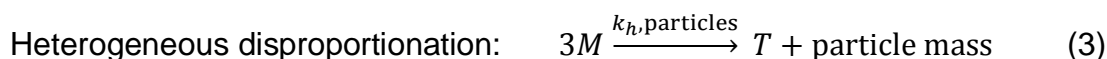
2 Review of the mathematical model

In this section, we briefly review the mathematical model developed by Kumar et al. (2007) for the GNPs synthesis by the citrate method. The model comprises material balance equations for the reactants and the products involved in the synthesis and a population balance equation (PBE) that describes how the particle size distribution (PSD) of the nanoparticles evolves. Before reporting such equations, we first clarify what compounds are present and what chemical reactions occur.

Chemical reactions

The components accounted for in the model are auric ions, citrate ions, aurous ions, dicarboxy acetone and acetone, represented by T, C, M, S and D, respectively. All the other reaction products are lumped in one fictitious component P. Five chemical steps are present:





Reaction 1 yields the reactants required in the subsequent steps. The reaction rate is assumed to be first-order with respect to both reactants. The reaction yields aurous ions and dicarboxy acetone.

From the Turkevich organizer theory, dicarboxy acetone organizes aurous ions in the nucleation step (reaction 2). This step requires two molecules of dicarboxy acetone to organize three aurous ions. When a sufficient number of aurous ions are brought together, they disproportionate to form a nucleus. The reaction rate is assumed to be third-order and second-order with respect to aurous chloride and dicarboxy acetone, respectively. Kumar et al. (2007) assumed that the nucleus has a known volume v_0 , thus containing ρv_0 moles of gold, where ρ denotes the molar density of gold. This step stops when either dicarboxy acetone or aurous ions are no longer available.

While step 2 occurs, so does step 3, which leads to particle growth. However, to take place, the latter requires the surface of particles. Thus, this step cannot occur before nuclei are formed. Steps 2 and 3 compete for aurous ions. For reaction 3, the rate is assumed to be first-order with respect to aurous chloride. As we will see in Section 4, unless a significant particle concentration is present in the system, the consumption rate of aurous ions by step 3 is negligible compared to that of step 2, the latter step being present until dicarboxy acetone (the catalyst for step 2) is fully degraded. This mechanism makes it possible to decouple nucleation from particle growth.

Reaction 4 represents the degradation of dicarboxy acetone. As mentioned, this step is crucial, since it limits nucleation and allows decoupling it from particle growth. The reaction rate is assumed to be first-order.

Reaction 5 occurs when the ratio of citrate to chloroauric acid is below unity. Acetone acts as a second reducing agent, converting the precursor into GNPs. The reaction rate is assumed to be first-order with respect to both reactants. In the model of Kumar et al. (2007), the stoichiometric coefficient of component T is 4, whereas we have used the value 2.5. The reason is explained in Appendix A of the Supporting Information (SI). The value 4 reported in the original model may be a typo. However, our simulations showed that, for the conditions investigated, the change in value of the coefficient does not affect the results significantly (in particular, the PSD and the mean size of the particles vary negligibly). As we will see in Section 4, reactions 2 and 4 determine the mean size. Because reaction 5 is much slower than these two reactions, varying the coefficient affects negligibly the mean size.

Table 2.1 summarizes the chemical reactions, along with their kinetic rate equations and constants (Section 3 reports how the values of the latter were obtained).

Balance equations

Assuming that the reaction solution is perfectly mixed (which implies that all intensive properties, such as temperature and concentrations, are uniform), we can select as control volume the region (of constant volume V) occupied by the mixture contained in the batch reactor in which the synthesis occurs. The material balance equations of the mixture components are then those reported below.

Auric chloride

This is reduced by citrate in step 1 and may be reduced by acetone in step 5. On the other hand, it is produced when aurous ions disproportionate in the nucleation and in the growth steps. The material balance equation is:

$$\frac{dC_T}{dt} = -k_c C_T C_C - k_d C_T C_D + k_n \rho v_0 C_M^3 C_S^2 + k_h C_M \int_{v_0}^{\infty} v^{2/3} P(v) dv \quad (2.1)$$

where C denotes the molar concentration of the reactants (the subscript indicating which component is being considered), k the reactions rate constants (the subscript indicating which reaction is being considered), v the nanoparticle volume (notice that this is not a constant, but a variable characterizing the internal state of the particles) and $P(v)$ the particle size distribution (this, in addition to the independent variable v shown explicitly, depends on the time as well).

Citrate

Citrate appears only in step 1 as a reactant. The material balance equation is:

$$\frac{dC_C}{dt} = -k_c C_T C_C \quad (2.2)$$

Aurous chloride

This is produced in steps 1 and 5, when auric chloride is reduced, but is consumed in steps 2 and 3. Therefore, the material balance equation is:

$$\frac{dC_M}{dt} = k_c C_T C_C + k_d C_T C_D - 3k_n \rho v_0 C_M^3 C_S^2 - 3k_h C_M \int_{v_0}^{\infty} v^{2/3} P(v) dv \quad (2.3)$$

Dicarboxy acetone

This is consumed by the reaction in step 4 and generated by the reaction in step 1. Note that in the nucleation step dicarboxy acetone acts as a catalyst, and therefore it is not consumed. The material balance equation is:

$$\frac{dC_S}{dt} = k_c C_T C_C - k_s C_S \quad (2.4)$$

Acetone

The material balance equation for acetone is obtained similarly and reads:

$$\frac{dC_D}{dt} = k_s C_S - (1/2.5) k_d C_T C_D \quad (2.5)$$

Gold nanoparticles

We describe the particle population using the number density function (NDF) $P(v, t)$, which is the number of GNPs per unit volume of physical and particle-volume space at time t . In other words, $P(v, t)$ is defined so that $P(v, t) dv$ represents the number of particles per unit volume of physical space with volume in the range dv around v at time t . The evolution of $P(v, t)$ is governed by the population balance equation and reflects the effects of the nucleation, growth and aggregation processes taking place in the mixture. The nucleation and growth rates are modelled as follows:

$$J_{nuc}(v) = 2k_n C_M^3 C_S^2 \delta(v - v_0) \quad (2.6)$$

$$G_v(v) = 2 \frac{k_h}{\rho} C_M v^{2/3} \quad (2.7)$$

where $\delta(v - v_0)$ is a Dirac delta function centered on the nucleus volume v_0 . The factor 2 on the right-hand side of the equations above appears because in reactions 2 and 3, for each mole of T that forms, two moles of gold atoms generate.

Although the model is based on a nucleation-growth mechanism, it accounts also for aggregation, in light of the experimental results that Chow and Zukoski (1994) found at high citrate concentrations. So, the aggregation submodel plays an important role only under some process conditions (clarified in Section 4), and is given by:

$$B(v) - D(v) = \frac{1}{2} \int_{v_0}^v \frac{q(v-v',v')}{W} P(v-v') P(v') dv' - P(v) \int_{v_0}^{\infty} \frac{q(v,v')}{W} P(v') dv' \quad (2.8)$$

The first and second terms represent particle birth and death caused by aggregation, respectively. q and W are the aggregation kernel and stability factor, respectively. The former is given by:

$$q(v, v') = \frac{2K_B T}{3\mu} \left(\frac{1}{v^{1/3}} + \frac{1}{v'^{1/3}} \right) \left(v^{1/3} + v'^{1/3} \right) \quad (2.9)$$

where K_B , T and μ are the Boltzmann constant, the temperature of the mixture and the viscosity of the fluid, respectively. The stability factor is given by the expression reported below. We discovered a typo in the equation for W reported by Kumar et al. (2007). The authors confirmed (via email correspondence) that the correct expression is:

$$\ln W = \frac{560}{\varphi} \log_{10} \left[(3C_{C_0} + C_{T_0}) \times 10 \right] + 27.5 \quad (2.10)$$

where C_{T_0} and C_{C_0} are the initial molar concentrations of chloroauric acid and sodium citrate, respectively, and φ is the surface charge, given by:

$$\varphi = -90[f + 1.5(1 - f)] \quad ; \quad f = \frac{1}{1 + 0.1C_C / (C_T + C_M)} \quad (2.11)$$

Note that W depends on C_{T_0} and C_{C_0} . These are the initial concentrations of T and C, and so do not change with time. The only variable in eq. (2.10) is φ , which can assume a maximum numerical value of -90 when $f = 1$ and a minimum numerical value of -135 when $f = 0$. Thus, $560/\varphi$ varies from -6.22 to -4.15 ; the order of magnitude does not change, and W changes little as the synthesis progresses. This

is unexpected. Rather, W should increase significantly and tend to infinity with time so as to stabilize the particles and prevent them from aggregating indefinitely.

Finally, the population balance equation reads:

$$\partial_t P(v) = -\partial_v [G_v(v)P(v)] + J_{nuc}(v) + B(v) - D(v) \quad (2.12)$$

The first term on the right-hand side of the equation models, as usual, convection; in this case, however, it is convection in particle-volume space (not in real space). The other three terms represent generation owing to nucleation and aggregation. For further details about the expressions reported above, we refer to Kumar et al. (2007).

3 Model implementation in Parsival

As shown, the model comprises material balance equations for the reacting species and a population balance equation for the GNPs. The former are ordinary differential equations, while the latter is an integro-differential equation. Their combination yields a complex model that can only be solved numerically. To this end, we employed a commercial code called Parsival. This simulation tool is designed for the integration of population balance equations in which the number density function representing the particle population, as well as any other intensive variable such as concentration, are uniform in space. However, the number density function adopted in Parsival is in terms of the particle diameter s , while the NDF in the original model of Kumar et al. is in terms of the particle volume v . Also, Parsival works on mass basis and expresses the material balances in terms of mass per unit time, while the original model is on mole basis and expresses the material balances in terms of moles per unit time. So, to solve the model in Parsival, we had to modify the equations. These are reported below (details about the conversion are given in Appendix B of SI). In the equations, Y is the molecular weight (the subscript indicating the component being considered) and $f(s, t)$ is the number density function in terms of the particle diameter s .

Auric chloride

$$\frac{d[C_T Y_T V]}{dt} = Y_T V \left[-k_c C_T C_C - k_d C_T C_D + k_n \rho v_0 C_M^3 C_S^2 + k_h m_v C_M \int_{s_0}^{\infty} s^2 f(s, t) ds \right] \quad (3.1)$$

Citrate

$$\frac{d[C_C Y_C V]}{dt} = -Y_C V [k_c C_T C_C] \quad (3.2)$$

Aurous chloride

$$\frac{d[C_M Y_M V]}{dt} = Y_M V \left[k_c C_T C_C + k_d C_T C_D - 3k_n \rho v_0 C_M^3 C_S^2 - 3k_h m_v C_M \int_{s_0}^{\infty} s^2 f(s, t) ds \right] \quad (3.3)$$

Dicarboxy acetone

$$\frac{d[C_S Y_S V]}{dt} = Y_S V [k_c C_T C_C - k_s C_S] \quad (3.4)$$

Acetone

$$\frac{d[C_D Y_D V]}{dt} = Y_D V \left[k_s C_S - \frac{1}{2.5} k_d C_T C_D \right] \quad (3.5)$$

All other products

$$\frac{d[C_P Y_P V]}{dt} = Y_P V \left[\frac{1}{2.5} k_d C_T C_D \right] \quad (3.6)$$

Population balance equation

$$\partial_t f(s) = -\partial_s [G_s(s) f(s)] + J_{nuc}(s) + B(s) - D(s) \quad (3.7)$$

with:

$$J_{nuc}(s) = 2k_n C_M^3 C_S^2 \delta(s - s_0) \quad (3.8)$$

$$G_s(s) = \frac{2}{3} \frac{k_h}{m_v^{1/3}} \frac{C_M}{\rho} \quad (3.9)$$

$$B(s) = \frac{1}{2} \int_{s_0}^s \frac{\alpha(\xi, s')}{W} \frac{s'^2}{\xi^2} f(s', t) f(\xi, t) ds' \quad \text{with} \quad \xi \equiv (s^3 - s'^3)^{1/3} \quad (3.10)$$

$$D(s) = f(s, t) \int_{s_0}^{\infty} \frac{\alpha(s, s')}{W} f(s', t) ds' \quad (3.11)$$

$$\alpha(s, s') = \frac{2k_B T}{3\mu} \left(\frac{1}{s} + \frac{1}{s'} \right) (s + s') \quad (3.12)$$

where m_v is the particle volume shape factor (which we set equal to $\pi/6$, assuming that the particles are spherical).

The nucleation term in the PBE involves a Dirac delta function. This function cannot be implemented in Parsival; therefore, we resorted to a similar but smooth function: a Gaussian distribution with mean equal to s_0 (that is, the size assumed for the nuclei) and an extremely small standard deviation.

In the synthesis no nanoparticles are initially present. We could implement this initial condition in Parsival, but an initial NDF that is identically zero may lead to numerical convergence problems. So, we initialized the problem employing the same Gaussian distribution used for modelling nucleation, making sure that the mass (or number) of particles initially present was vanishingly small and thus irrelevant.

We will show that these assumptions (i.e., initial particle mass and initial form of the NDF) do not affect the results.

4 Implementation check

To check that the model had been correctly implemented in Parsival, we reproduced some of the results obtained by Kumar et al. (2007). Parsival requires values for the seven parameters used in the model, i.e., k_h , k_n , k_s , k_d , k_c , ρ and v_0 . Kumar et al. (2007) obtained the values for k_h , k_n and k_s via best-fit, by requiring that the model

results should fit the data of Frens (1973). They fixed k_c to render the synthesis time of the same order of magnitude as that experimentally determined at 100 °C. Also, they assumed a value for k_d smaller than k_c to reflect that the time the process takes to complete is larger when a limited amount of citrate is present (as opposed to the case in which citrate is in excess). They took the value of ρ from the literature and assumed a nucleus size of 2 nm. We employed the same values in our simulations. These are:

$$k_c = 1.25 \frac{m^3}{mol \cdot s} \quad ; \quad k_n = N_{av} 1.67 \times 10^{-3} \left(\frac{m^3}{mol} \right)^5 \frac{1}{m^3 \cdot s} \quad ; \quad k_s = 1 \frac{1}{s}$$

$$k_h = 2.5 \times 10^{-4} \frac{m^3}{m^2 \cdot s} \quad ; \quad k_d = 4 \times 10^{-1} \frac{m^3}{mol \cdot s}$$

$$\rho = 1 \times 10^5 \frac{mol}{m^3} \quad ; \quad v_0 = 4.18 \times 10^{-27} m^3$$

From these values, we obtained approximate characteristic times for the various reactions of the synthesis (see Appendix C in the SI). The synthesis begins with the reduction of chloroauric acid by citrate (reaction 1), which produces aurous chloride and dicarboxy acetone. The characteristic time of this reaction is $\tau_c \sim 10$ s. In the presence of dicarboxy acetone, aurous chloride converts according to reaction 2, whose characteristic time is $\tau_n \sim 10^4$ s. Concurrently, dicarboxy acetone degrades into acetone according to reaction 4, whose characteristic time is $\tau_s \sim 1$ s. Once dicarboxy acetone is consumed, reaction 2 stops. Therefore, reaction 2 has barely started when it stops. However, quite a lot of nuclei are formed ($\sim 10^{17}$ nuclei/ m^3). According to reaction 3, the residual aurous chloride grows the formed nuclei. The characteristic time of this reaction is $\tau_h \sim 10^2$ s. The last reaction is the second reduction of auric chloride by acetone, occurring only when the ratio of citrate to chloroauric acid is less than unity. The synthesis, nevertheless, is usually carried out with citrate in excess, and therefore we did not estimate the characteristic time of this final reaction.

As previously pointed out, the model also accounts for aggregation; nevertheless, particles only aggregate significantly under certain conditions. We will point out these conditions when discussing how the model predicts the data of Chow and Zukoski (1994). Before that, we discuss the results from the simulations obtained by using the initial conditions adopted previously by Frens (1973) and subsequently by Kumar et al. (2007). The latter, Case 1, will illustrate that in the Turkevich organizer theory particles evolve via the nucleation and growth processes; the former, Case 2, will illustrate the conditions that favour aggregation. In reporting the experimental data, we included error bars only for the data of Chow and Zukoski (1994), because the other researchers did not report them in their publications.

Case 1

Kumar et al. (2007) employed the experimental data of Frens (1973), which were obtained by keeping C_{T_0} constant at 0.3 mol/m^3 while changing C_{C_0} from 0.12 to 0.76 mol/m^3 at 100°C . These initial conditions translate into citrate to gold ratios from about 0.4 to 2.5. They reported their numerical solutions (the mean diameter of the particles) when 99% of gold had converted to GNPs, basing this criterion on the fact that the first and higher-order processes included in the model take infinite time to complete (Kumar et al., 2007). In the simulations, for the case where $C_{T_0} = C_{C_0} = 0.3 \text{ mol/m}^3$, this criterion translated into a synthesis time of $\sim 10^2 \text{ s}$. The synthesis times for other cases may be longer or shorter, depending on the initial conditions.

Figure 4.1 reports the numerical predictions obtained by us in Parsival and by Kumar et al. (2007), along with the experimental findings of Frens (1973). Kumar et al. extended the numerical predictions beyond a ratio of 2.5, considering values up to 7. Our predictions agree reasonably well with those of Kumar et al., with a maximum deviation within 5%. To illustrate how we obtained this agreement, let us analyse the results further. For the case in which $C_{T_0} = C_{C_0} = 0.3 \text{ mol/m}^3$, the characteristic time for aggregation ($\sim 10^8 \text{ s}$) is much longer than the synthesis time ($\sim 10^2 \text{ s}$). Therefore, aggregation is insignificant, and the mean size of the particles is 48 nm , as reported by Kumar et al. The particles form at 2 nm (the nucleus size) and then grow to their final size. We can calculate the amount of gold that forms the nuclei as follows:

$$\frac{\text{amount of gold for both nucleation and growth}}{\text{amount of gold for nucleation only}} = \frac{0.3}{x} = \frac{48^3}{2^3} \rightarrow x = 2.17 \times 10^{-5} \text{ mol/m}^3 \quad (4.1)$$

Thus, the nuclei concentration that Kumar et al. obtained is:

$$\frac{x}{\rho v_0} = \frac{2.17 \times 10^{-5} \text{ mol/m}^3}{1 \times 10^5 \text{ mol/m}^3 \times 4.18 \times 10^{-27} \text{ m}^3} = 5.19 \times 10^{16} \text{ nuclei/m}^3$$

In our simulations we obtained $5.23 \times 10^{16} \text{ nuclei/m}^3$ (the relative deviation from the value above is less than 0.8%). Because these values are very close, our predictions closely agree with those of Kumar et al.

Citrate reacts with auric ions to produce aurous ions and dicarboxy acetone. The stoichiometric ratio of citrate to gold, obtained by combining reactions 1 to 5, is 1.5 (refer to Kumar et al., 2007). DCA organizes the aurous ions in the nucleation step (reaction 2), but concurrently degrades into acetone (reaction 4). When C_{C_0}/C_{T_0} is less than 1.5, the amount of DCA is limited by the concentration of citrate. Thus, as this ratio decreases, the rate of nucleation decreases. Because the concentration of the precursor is kept constant, the nuclei produced grow to bigger sizes.

When C_{C_0}/C_{T_0} is higher than 1.5, the amount of DCA is limited by the concentration of chloroauric acid, which is kept constant. Hence, as the ratio increases, the rate of nucleation remains almost constant, yielding GNPs of almost identical mean size.

Case 2

Kumar et al. (2007) used this case to emphasize the role of aggregation, which was insignificant for the conditions examined above. The experimental results that they tried to reproduce were those of Chow and Zukoski (1994). The latter varied C_{T_0} from 0.02 to 1.26 mol/m^3 while keeping C_{C_0} and the temperature constant at 1.60 mol/m^3 and 70°C , respectively, and reported that the nanoparticles aggregated. Although the temperature was different from Case 1, Kumar et al. used the same values of the reaction rate constants. In our investigation, we did the same, not accounting for the temperature effect, inasmuch as our goal in this preliminary part of the work was to reproduce the values reported by Kumar et al. and discuss our findings.

With these conditions citrate is always in excess, so that chloroauric acid determines the amount of DCA formed. Using the same criterion of 99% of gold converted to GNPs and following the reasoning in Appendix C of the SI, the synthesis times for $C_{T_0} = 0.1 \text{ mol/m}^3$ and $C_{T_0} = 1.26 \text{ mol/m}^3$ are $\sim 10^3 \text{ s}$ and $\sim 10 \text{ s}$, respectively. Figure 4.2 shows the predictions of the model that we implemented and those obtained by Kumar et al., compared with the experimental data of Chow and Zukoski (1994). The model of Kumar et al. does not match the experimental data very well; however, the results seem to yield a correct trend, showing that the mean diameter decreases to a minimum value and then increases when the initial concentration of tetrachloroauric acid is increased. This, as Kumar et al. reported, shows that the aggregation process observed by Chow and Zukoski does occur. The predictions of the model which we implemented in Parsival, however, do not show this trend (see Figure 4.2 for the predictions trend at 99% of gold converted to GNPs).

To investigate the reason for this difference, we estimated the characteristic times of the aggregation process for $C_{T_0} = 0.1 \text{ mol/m}^3$ and $C_{T_0} = 1.26 \text{ mol/m}^3$. The times we obtained are $\tau_a \sim 10^9 \text{ s}$ and $\tau_a \sim 10^3 \text{ s}$, respectively (refer to Appendix D of the SI for details). At these lowest and highest initial concentrations of tetrachloroauric acid, the characteristic times of aggregation (10^9 and 10^3 s) are much longer than the corresponding synthesis times (10^3 and 10 s , respectively). We therefore concluded that the results reported by Kumar et al. in this case could not be obtained using the 99% conversion criterion previously described.

When $C_{T_0} = 0.1 \text{ mol/m}^3$ (the lowest initial concentration of tetrachloroauric acid), the citrate to gold ratio is 16. In these conditions, about $4 \times 10^{14} \text{ nuclei/m}^3$ form, hence consuming $1.7 \times 10^{-7} \text{ mol/m}^3$ of auric ions (see Appendices C and D of the SI for details). These nuclei grow to an estimated mean particle diameter of 168 nm (this value is not shown in Figure 4.2). For the highest initial concentration of tetrachloroauric acid, however, $C_{T_0} = 1.26 \text{ mol/m}^3$, about $1.3 \times 10^{20} \text{ nuclei/m}^3$ form, thus consuming $5.34 \times 10^{-2} \text{ mol/m}^3$ of auric ions. These nuclei grow to an estimated mean particle diameter of 5.65 nm . Hence, within the synthesis time, the particle diameter decreases when the initial concentrations of tetrachloroauric acid increase. This agrees with our numerical results.

To obtain the trend reported by Kumar et al., we ran the simulation for much longer times than the synthesis times to allow particles to aggregate. The model predictions

at different simulation times (10^6 , 10^7 and 5×10^7 s) are also shown in Figure 4.2. Since the characteristic time for aggregation at $C_{T_0} = 1.26 \text{ mol/m}^3$ is 10^3 s, by 10^6 s the NPs have started to aggregate, increasing the mean particle diameter from 4.96 nm to 10.3 nm. As C_{T_0} decreases, the particle concentration decreases while τ_a increases, the particles requiring longer times to aggregate significantly. By 10^6 s, the mean size for $C_{T_0} = 1.26 \text{ mol/m}^3$ has increased to more than twice the value obtained at 99% gold converted to particles; conversely, for $C_{T_0} = 0.42 \text{ mol/m}^3$, for instance, the mean size has only increased from 12.5 nm to 13.2 nm.

We should note that in the model of Kumar et al. particles aggregate indefinitely; this is because the stability factor W , which should increase with time, remains constant. As shown in Section 2, W depends on the *initial* concentrations C_{T_0} and C_{C_0} , not on the current concentrations C_T and C_C . Figure 4.2 reveals this indefinite aggregation: the longer the simulation time, the larger the mean particle diameter. We can infer that, as the simulation time tends to infinity, the particles would coalesce into one aggregate. This is clearly at variance with the experimental evidence.

To make the model correctly reflect the experimental evidence, which indicates that aggregation must eventually stop, in the equation for the stability factor, Eq. (2.10), we replaced the initial concentrations, C_{T_0} and C_{C_0} , with the current ones, C_T and C_C . The model, however, did not improve. As C_T and C_C decrease due to the reactions, W , and in turn the aggregation time, increase. Because C_T and C_C eventually reach constant values (but do not both vanish), W and the aggregation time also reach constant values. Accordingly, the aggregation time never diverges and the particles aggregate indefinitely at constant rate. However, several authors, such as Chow and Zukoski (1994) and Ji et al. (2007), reported that the aggregation process becomes less significant as particle size increases. Therefore, the expression for W must be a function of, and should increase with, particle size.

Because particles aggregate indefinitely in the model, we retain the criterion of 99% of gold converted to GNPs to obtain the simulation time and use the corresponding mean size in testing the model in Section 5.

Effects of our assumptions in the model implementation

We ran four simulations to check the effect of the reactor volume and of the initial particle size distribution on the results of the model. In the model of Kumar et al. (2007), it was assumed that the system was perfectly mixed. This implies that the properties of the system are uniform in physical space and therefore do not depend on the location in physical space. It also implies that the reactor volume should not affect the results of the model. To check this, we varied the reactor volume, keeping the initial concentration of the reactants constant. We used two reactor volumes of 2 and 10 m^3 , respectively. To check the effect of the initial particle size distribution, we used two distributions of different shapes (see Figure 4.3), denoted as D1 and D2. In all cases, the initial particle mass was set to $1\text{e-}20$ kg; this is a negligible amount, which reflects the fact that initially no particles are really present in the system (note that, as already mentioned, using an initial distribution that vanishes identically over

the entire size space is not recommended). In all cases, the final mean size of the particle was the same, equal to 46.5 nm. So, as expected, neither the volume nor the shape of the initial distribution affects the numerical results.

5 Testing of the model

In the previous sections, we reported and solved the model developed by Kumar et al. (2007); also, we compared our results to those of Kumar et al. (2007). In this section, we test the model using experimental data available in the literature to assess whether the Turkevich organizer theory, on which the model is based, rightly describes the synthesis. Kumar et al. used the discussions in Case 1 (Section 4) to illustrate that the organizer theory is generally valid for the citrate reduction method. After employing the work of Frens (1973) to estimate the parameters used in the model and predicting his experimental data with excellent agreement, Kumar et al. reported that the same model parameters gave good predictions for the work of Turkevich et al. (1951), Freund and Spiro (1985), and Abid (2003). We believe the model well reproduced these data because these researchers used initial conditions similar to those of Frens, whose work Kumar et al. fitted to make the predictions from the nucleation-growth model accurate. In Case 2 we showed how the model failed to predict the data of Chow and Zukoski (1994) and the inconsistencies in temperature and simulation times. In this section, we employ new data to test the model.

Many other researchers have investigated the synthesis experimentally and in recent times have emphasized the significant role of pH in the synthesis (both the initial and final pH), which determines how particles evolve in the synthesis. For example, Ji et al. (2007) observed that NPs evolve by nucleation, aggregation and growth when the final pH of the mixture is below 6.5, while they evolve by nucleation and growth when the final pH of the mixture is above 6.5. In the same way, Wuithschick et al. (2015) stated that the synthesis follows the seed-mediated mechanism (which is consistent with the nucleation-aggregation-growth description of the synthesis) when the initial pH is equal to 3.5. This mechanism of the synthesis can be explained on the basis of the chemical properties of the precursor and reducing agent, which are a strong acid and a weak base, respectively.

The precursor, tetrachloroauric acid, completely ionizes in an aqueous solution to release hydrogen ions and tetrachloroauric ions. In the presence of a base, hydroxyl ions replace chloride species in tetrachloroauric ions to yield from monohydroxylated to tetrahydroxylated species. The speciation of the latter depends on the pH. The more hydroxylated the species is, the less reactive it is [whilst monohydroxylated trichloroauric ions can be reduced, species from dihydroxylated dichloroauric ions do not react, unless the pH is lowered (Ji et al., 2007)]. The model developed by Kumar et al. (2007) does not account for these pH effects, solely accounting for how the tetrachloroauric acid reduces in the synthesis.

The reducing agent, on the other hand, performs three important roles: reduces the precursor, supplies the hydroxyl ions and stabilizes the NPs, preventing aggregation. These additional reactions and processes render the synthesis complex to describe.

Wuithschick et al. (2015) identified the factors affecting the final size as temperature, the initial concentrations of the precursor and reducing agent, and the initial and final pH. Thus, we used these factors to test the model. First, we tested the model against the work of Wuithschick et al. (2015) and Turkevich et al. (1951) for the effect of temperature. Second, we tested it against the work by Takiyama (1958), carried out at 80 °C. Third, we employed the works of Zabetakis et al. (2012) and Li et al. (2011) to test the model for the effect of the initial pH of the precursor. Lastly, we used the data of Ji et al. (2007) to test the role of the final pH of the mixture. For all these experimental data, we did not report error bars, because they were unavailable in the articles mentioned above, from which the data were taken.

5.1 Effect of temperature

In their publication, Kumar et al. (2007) only tested the model for the Turkevich organizer theory at the usual synthesis temperature of 100 °C. In the literature, however, authors such as Turkevich et al. (1951) and Wuithschick et al. (2015) have investigated the effect of temperature on the final particle diameter. The former reported the mean sizes at 70, 80 and 100 °C for initial concentrations of $C_{T_0} = 0.26 \text{ mol/m}^3$ and $C_{C_0} = 1.9 \text{ mol/m}^3$, while the latter reported the mean sizes as the temperature changed from 23 to 100 °C for initial concentrations of $C_{T_0} = 0.25 \text{ mol/m}^3$ and $C_{C_0} = 2.5 \text{ mol/m}^3$. In both cases, citrate was in excess. To test the model at temperatures different from 100 °C, we require the activation energies for the reactions involved in the synthesis so as to obtain their corresponding reaction rate constants. Out of five reactions, only four have their activation energies reported in the literature. Turkevich et al. (1951) reported the activation energies for the nucleation step (reaction 2) and growth step (reaction 3) as 10 and 9.1 kcal/mol respectively; Wiig (1928) reported an activation energy for the reaction of dicarboxy acetone decomposition (reaction 4) of 23.1 kcal/mol. Using molecular modelling, Ojea-Jiménez and Campanera (2012) obtained the activation energy of the reduction step by citrate (reaction 1) as 34 kcal/mol. The last reaction (reaction 5), as we discussed, occurs only when the ratio of the initial concentrations of sodium citrate to tetrachloroauric acid is below unity. Therefore, in these investigations, reaction 5 was insignificant.

Figure 5.1A shows how the mean particle diameter changes with temperature for the data of Wuithschick et al. (2015). The model poorly predicts the experimental data. Starting from 23 °C, the mean size from experiment decreases with temperature and reaches a minimum value at around 60 °C before increasing. In contrast, the model predicts that the size decreases from 23 °C, where the mean diameter is 24.5 nm, to 40 °C, where the mean diameter is 21.5 nm, remaining constant thereafter. In this range of temperatures, the characteristic time of aggregation remains essentially constant at 10^7 s (see Appendix D of the SI for details). However, the synthesis time decreases with increasing temperature. At 23 °C, the synthesis time is 10^9 s , a value obtained following the reasoning in Appendix C of the SI, where the reaction rate constants at this temperature are used. As the synthesis time is longer than the time constant for aggregation, the particles aggregate, attaining a final mean size of 24.5

nm. At higher temperature, the effect of aggregation decreases as the synthesis time decreases. Therefore, the mean size decreases. By 50 °C, aggregation has stopped affecting the mean size, because the synthesis time is now much shorter than the characteristic time of aggregation. When the effect of aggregation is negligible, as highlighted in Section 4, the balance between the nucleation step (reaction 2) and the decomposition of dicarboxy acetone (reaction 4) determines the final mean size, which remains constant at 21.3 nm with increasing temperature. To explain this profile, in Table 5.1, we report the values of the rate constants of reactions 2 and 4, and their ratio at different temperatures. The ratio (k_r/k_s) remains constant, and this explains why the final mean size is constant as well. However, the experimental data do not remain constant with temperature; so, the balance between reactions 2 and 4 does not describe the synthesis. This aspect, consequently, is not properly captured by the model of Kumar et al. The primary reason for this is that the stability factor W depends on the temperature of the mixture (Chow and Zukoski, 1994; Marchisio and Fox, 2013), but in the constitutive equation for particle aggregation used in the model of Kumar et al. this dependence is not accounted for.

The seed-mediated mechanism proposed by Wuithschick et al. (2015) describes the synthesis and explains the profile of the final mean size with temperature shown in Figure 5.1A. According to this mechanism, nuclei generate after citrate reduces tetrachloroauric acid. These nuclei aggregate to form bigger particles. Similarly, particles containing two or more nuclei can also aggregate. Nevertheless, particle aggregation stops for particles with sizes equal to the seed size [see Wuithschick et al. (2015) for more information]. The seeds subsequently grow to the final particle size. Thus, the seed-mediated mechanism occurs according to the order nucleation, aggregation and growth. Among these processes, aggregation is the most sensitive to temperature. Temperature affects both the aggregation kernel q and the stability factor W , both of which determine the aggregation rate (Marchisio and Fox, 2013). For an aqueous system, Wang et al. (2010) reported that aggregation is insignificant below 60 °C for the reaction conditions which Wuithschick et al. (2015) investigated. Temperature also affects the rates of the nucleation and growth processes, as the Arrhenius equation illustrates. At low temperatures, both rates decrease so that only few nuclei form, and these grow slowly. Since the reaction mixture is left until all the precursor is converted, the few nuclei formed at 23 °C reach a large final size. As the temperature increases from 23 to 60 °C, the nucleation rate increases, forming more nuclei and leaving behind a smaller amount of precursor. The latter grows the many nuclei to smaller final sizes. For these initial conditions, as observed in Figure 5.1A, aggregation becomes significant above 60 °C. As the temperature rises from 60 °C, particle aggregation increases the final particle size.

5.2 Effect of initial HAuCl_4 concentration

Another investigation of the Turkevich synthesis that did not follow the usual method of changing citrate concentration at a fixed concentration of tetrachloroauric acid was that by Takiyama (1958). This investigation predated the work of Frens and provides additional data with which to test the model. Takiyama studied the synthesis at 80 °C

and $C_{C_0} = 3.88 \text{ mol/m}^3$ while changing C_{T_0} from 0.05 to 1.28 mol/m^3 ; so, citrate is in excess. In solving the model for these initial conditions, we used the values of the reaction rate constants and other parameters at the operating temperature. Figure 5.2 shows the model predictions along with the corresponding experimental data. For the model predictions, which do not agree with the data, the profile of the mean particle diameter with the initial concentration of gold resembles that of Figure 4.2 (this was expected, because the operating conditions in this study resemble those of Case 2, discussed in Section 4). As the synthesis is at 80°C , the synthesis time is far shorter than the aggregation characteristic time, so that the role of aggregation is negligible and only nucleation and growth affect the particle size distribution. If we assume that the two latter processes are fully decoupled (as shown in Section 4), the concentration of nuclei formed equals the concentration of particles in the final reaction mixture. As revealed in Appendix D of the SI, to determine the concentration of nuclei N_c , we need to know the maximum concentration of nuclei $N_{c,max}$, the characteristic time for nucleation τ_n and the characteristic time for the decomposition of dicarboxy acetone τ_s . The expression $N_c = (\tau_s/\tau_n)N_{c,max}$ is found. If we consider the lowest concentration of precursor considered, $C_{T_0} = 0.05 \text{ mol/m}^3$, following the reasoning presented in Appendix C of the SI, we obtain $\tau_s = 10 \text{ s}$, $\tau_n = 10^6 \text{ s}$ and $N_{c,max} = 7.97 \times 10^{19} \text{ nuclei/m}^3$, which results into $N_c = 4.26 \times 10^{14} \text{ nuclei/m}^3$. This estimate has of the same order of magnitude as the value obtained from the model numerical solution ($2.13 \times 10^{14} \text{ nuclei/m}^3$). In forming these nuclei, $\rho v_0 N_c = 1.78 \times 10^{-7} \text{ mol/m}^3$ of the precursor converts. The concentration of the precursor that is left is $\sim 0.05 \text{ mol/m}^3$. Using Eq. (4.1), the remaining amount grows the nuclei to:

$$\sqrt[3]{\left(\frac{0.05}{8.9 \times 10^{-8}} \times 2^3\right)} = 165 \text{ nm}$$

For the highest precursor concentration, $C_{T_0} = 1.28 \text{ mol/m}^3$, on the other hand, the model numerical solution yields a nuclei concentration of $3.32 \times 10^{20} \text{ nuclei/m}^3$, which is $\sim 10^6$ times the concentration of nuclei obtained for $C_{T_0} = 0.05 \text{ mol/m}^3$. These more concentrated nuclei grow to a mean size of 3.4 nm . Thus, as we move from $C_{T_0} = 0.05 \text{ mol/m}^3$ to 1.28 mol/m^3 , the mean particle diameter decreases from 165 nm to 3.4 nm .

The seed mediated mechanism, on the other hand, explains the experimental profile in Figure 5.2. The final mean size increases slightly from 15 nm at $C_{T_0} = 0.05 \text{ mol/m}^3$ to 19 nm at $C_{T_0} = 0.10 \text{ mol/m}^3$ and then remains almost constant afterwards. Because the sodium citrate solution can supply OH^- , the precursor can undergo two reactions: reduction to form the nuclei and passivation by OH^- . The passivation can produce monohydroxylated species of the precursor; even in the presence of much OH^- , it can produce higher hydroxylated species of the precursor. The monohydroxylated species reduces to gold and grows the particles while the higher hydroxylated species cannot reduce to gold, leaving behind unconsumed gold in the solution. At $C_{T_0} = 0.05 \text{ mol/m}^3$, the ratio of citrate to gold is 80, producing much OH^- that can form higher hydroxylated species. The mean size is small as some of the

precursor is lost to the formation of higher hydroxylated species. As C_{T_0} increases, the ratio of citrate to gold decreases, producing a smaller amount of OH^- . Therefore, more precursor converts to gold nanoparticles, increasing the mean size. As C_{T_0} increases further, more precursor goes through the reduction step and produces many nuclei and seeds. Although more precursor also forms the monohydroxylated species that can grow the seeds, the balance between the number of seeds and the amount of gold available to grow them keeps the final mean size almost constant.

5.3 Effect of initial pH of $HAuCl_4$ (aq)

To test the effect of the initial pH of the precursor, we employed the initial conditions of the work by Zabetakis et al. (2012). They synthesized the NPs at different initial concentrations ($0.3 - 2.0 \text{ mol/m}^3$) of the precursor at a temperature of $100 \text{ }^\circ\text{C}$, keeping the citrate to gold ratio (denoted as R) constant. They considered R values of 2, 3, 4 and 5. We obtained the initial pH values from the initial concentrations of tetrachloroauric acid, which is a strong acid. Figure 5.3 shows the model predictions against the experimental data for the effect of the initial pH of tetrachloroauric acid for all the values of R investigated. The model predictions are unsatisfactory. They generally increase as the initial pH rises, unlike the experimental data that decrease and then increase, hence presenting a minimum. Low initial pH translates into high concentration of tetrachloroauric acid. For instance, for $R = 2$ (i.e., the lowest pH considered, equal to 2.93), $C_{T_0} = 1.2 \text{ mol/m}^3$. From the simulation, this concentration yields $\sim 10^{20} \text{ nuclei/m}^3$, consuming $4.18 \times 10^{-2} \text{ mol/m}^3$ of T . Since aggregation is insignificant, these nuclei can only grow to a mean size of 3.9 nm , consuming the remaining quantity of T . The highest pH of 3.53, on the other hand, corresponds to $C_{T_0} = 0.3 \text{ mol/m}^3$, and generates $\sim 10^{18} \text{ nuclei/m}^3$. To form, these nuclei consume $4.18 \times 10^{-4} \text{ mol/m}^3$ of T and grow to a bigger mean diameter. So, in the numerical simulations, as the initial pH increases, the mean diameter increases.

The seed-mediated mechanism describes the behaviour observed experimentally. Low initial pH translates into a small amount of OH^- , which can only passivate a small portion of the precursor. Most of the precursor converts into gold and produces several nuclei. These nuclei aggregate to form the seeds. On how the reaction condition favours aggregation, Wuithschick et al. observed vigorous aggregation at low pH that becomes less significant as the initial pH increases. Thus, at low pH, because of the effect of aggregation, the several nuclei aggregate to form larger seeds, producing larger final particles. As the initial pH increases, the amount of OH^- , which passivates the precursor, increases. The amount of the precursor that converts into gold decreases, yielding fewer nuclei. Because aggregation becomes less significant, these fewer nuclei aggregate less into smaller seeds, producing final smaller particles. As the initial pH increases further, even more precursor becomes passive. A small portion of the precursor reduces to even fewer nuclei. However, according to Wuithschick et al., increasing the initial pH at this stage does not significantly reduce the seed size. Thus, the fewer nuclei yield fewer seeds. Then, the passive form of the precursor, which increases with the initial pH, grows the fewer seeds to larger particles.

Li et al. (2012) published a work similar to that of Zabetakis et al. (2012). They used different initial concentrations of tetrachloroauric acid at a constant citrate-to-gold ratio of 4. Figure 5.4 shows their data with the corresponding model predictions; the trends are similar to those reported by Zabetakis et al., and similar considerations to those already discussed hold.

5.4 Effect of final pH of the mixture

As previously mentioned, Ji et al. (2007) have reported that the mechanism of the synthesis depends on the final pH of the reaction mixture: at low pH the mechanism involves nucleation, aggregation and then growth, while at high pH it involves only nucleation and then growth. Calculating the final pH of the reacting mixture requires detailed knowledge of the thermodynamics of the synthesis, which is currently not available in the literature. The dissociation of sodium citrate depends on the pH, which in turn depends on the sodium citrate concentration. Along with reporting the values of the citrate to gold ratios considered, Ji et al. (2007) measured the corresponding final pH of the synthesis. They varied C_{C_0} from 0.23 mol/m^3 to 6.92 mol/m^3 while keeping both C_{T_0} and the temperature constant at 0.25 mol/m^3 and $100 \text{ }^\circ\text{C}$, respectively. Figure 5.5 shows their data along with the model predictions at 99% of gold converted to GNPs. With this criterion, aggregation is insignificant in the simulation. For the model predictions, as the final pH increases, the mean particle diameter decreases. While, for the experimental data, the mean particle diameter decreases until the final pH reaches 6.5 and then increases. The lowest final pH of 4.15 corresponds to $C_{C_0} = 0.23 \text{ mol/m}^3$ and a citrate to gold ratio $R = 0.9$. For this ratio, in the model, citrate is the limiting reactant and determines the amount of DCA that forms the nuclei. The concentration of the latter is $\sim 10^{17} \text{ nuclei/m}^3$. These nuclei then grow to a mean size of 71.6 nm . Increasing the final pH corresponds to increasing C_{C_0} so that citrate becomes in excess and C_{T_0} starts determining the amount of DCA that forms the nuclei. The highest final pH of 6.92 corresponds to $C_{C_0} = 6.92 \text{ mol/m}^3$. At this pH, $C_{T_0} = 0.25 \text{ mol/m}^3$ and the concentration of nuclei results to be $\sim 10^{19} \text{ nuclei/m}^3$, $\sim 10^2$ times larger than that of the lowest pH. The nuclei concentration therefore varies from $10^{17} \text{ nuclei/m}^3$ at the minimum final pH to $10^{19} \text{ nuclei/m}^3$ at the maximum final pH. As C_{T_0} is constant at 0.25 mol/m^3 , the final mean size decreases with increasing pH.

It is still the seed-mediated mechanism by Wuithschick et al. (2015) that explains the experimental data, just as Ji et al. (2007) also explained the synthesis in their report using two mechanisms: nucleation-aggregation-growth when the pH is below 6.5 and nucleation-growth when the pH is above 6.5. Both explanations, by Ji et al. (2007) and Wuithschick et al. (2015), stem from the acid-base properties of the precursor and reducing agent. From thermodynamics, tetrachloroauric ion converts reversibly to the monohydroxylated form, both ions being present in equal amounts at the pH of 6.5. pH below 6.5 shifts the equilibrium to tetrachloroauric ion while pH above 6.5 shifts it to the monohydroxylated form. At the lowest final pH of 4.15, almost all the precursor forms nuclei; only a small portion (or even none) of it becomes hydroxylated. This produces several nuclei that then aggregate to form large

particles. As the final pH increases, aggregation starts playing a less significant role, and therefore the particle diameter decreases until the final pH is 6.5. Above 6.5, less of the precursor forms nuclei while more becomes hydroxylated, so that less particles form, which later grow when the hydroxylated precursor reacts on the particle surface. Thus, the increase in size after the pH of 6.5 is due to fewer particles growing bigger, whereas the increase in size below the pH of 6.5 is due to several particles aggregating into bigger sizes.

6 Conclusions

This work investigated the mathematical model developed by Kumar et al. (2007) for the synthesis of gold nanoparticles by means of the citrate method. This is the only model, based on the Turkevich organizer theory, available in the literature. The model accounts for five reaction steps, one of which produces dicarboxy acetone, which organizes gold in the nucleation step. While DCA decomposes, the particles grow by the deposition of the residual precursor on their surfaces. GNPs evolve by the nucleation-growth mechanism, as proposed by Turkevich et al. (1951). Although Kumar et al. (2007) included a submodel for aggregation, this submodel does not play a significant role over the synthesis time.

Further, we tested the model for different conditions of temperature, concentrations and pH using various experimental data from the literature. The model performed poorly in describing the synthesis. We believe that this is because the five chemical steps over which the model of Kumar et al. is built do not reflect the chemistry of the synthesis accurately. Because the precursor and reducing agent are a strong acid and a weak base, respectively, their acid-base properties cover an important role in the synthesis. As a weak base, the reducing agent releases OH^- in water. The precursor, on the other hand, can be reduced and/or hydroxylated. Kumar et al. only modelled the reduction step that produces the nuclei but did not consider the hydroxylation step. Subsequently, these nuclei aggregate into seeds, which then grow by reacting with the hydroxylated precursor. Using the seed-mediated mechanism proposed by Wuithschick et al. (2015), we were able to qualitatively explain the experimental data reported by the researchers.

In the light of this work, it is necessary that a new model be derived for the citrate method. Since the seed-mediated mechanism of Wuithschick et al. (2015) seems to be able to convincingly describe the trends observed experimentally, this model should be based on this mechanistic theory along with all the chemical steps that reflect the acid-base properties of the precursor and reducing agent. The new model should therefore account for the hydroxylation of the precursor and its speciation, the simultaneous reduction of the precursor to gold atoms, the speciation of the reducing agent, the aggregation of gold atoms into seed particles, and the growth of the latter into the final GNPs via reaction with the hydroxylated form of the precursor.

Acknowledgments

The authors are grateful to Dr. Michael Wulkow, managing director of Computing in Technology GmbH (CiT), the company that developed the numerical code Parsival, for his support and the stimulating discussions.

Emmanuel Agunloye would also like to thank the Nigerian government for funding this research project via the Petroleum Trust Development Fund and the National University Commission.

Nomenclature

Symbol	Meaning	Units
Roman alphabets		
$B(v)$	Birth aggregation rate	$1/(dm^3 \cdot cm^3 \cdot s)$
C_T	gold (III) chloride	mol/m^3
C_C	Citrate	mol/m^3
C_D	Acetone	mol/m^3
C_M	aurous chloride	mol/m^3
C_S	Dicarboxy acetone	mol/m^3
C_P	Other products	mol/m^3
$D(v)$	Death aggregation rate	$1/(dm^3 \cdot cm^3 \cdot s)$
f	Fraction of surface occupied by gold species	—
$f(s)$	number of particles per particle-length per total volume of fluid-particle mixture	$1/(m^3 \cdot m)$
G_s	linear growth rate	m/s
G_v	volume-growth rate	m^3/s
J_{nuc}	Nucleation rate	$1/(m^3 \cdot s)$
k_c	Rate constant for the reaction between citrate and auric acid	$m^3/(mol \cdot s)$
k_d	Rate constant for the reduction with acetone	$m^3/(mol \cdot s)$
k_n	Rate constant for the	$(m^3)^4/(mol^5 \cdot s)$

	nucleation step	
k_s	Rate constant for the degradation of dicarboxy acetone	1/s
k_h	Rate constant for the growth step	m/s
K_B	Boltzmann constant	J/K
N_{av}	Avogadro's number = $6.02e23$	—
$P(v)$	number of particles per particle-volume per total volume of fluid-particle mixture	$1/(dm^3 \cdot cm^3)$
$q(v, v')$	Aggregation kernel	m^3/s
r	Kinetic rate equation	$mol/(m^3 \cdot s)$
s	Size	m
s_0	Smallest particle size	m
s_v	Particle size of volume v	m
t	Time	s
T	Temperature	K
v	Particle volume	m^3
V	total volume of the fluid-particle mixture	m^3
W	Stability factor	—

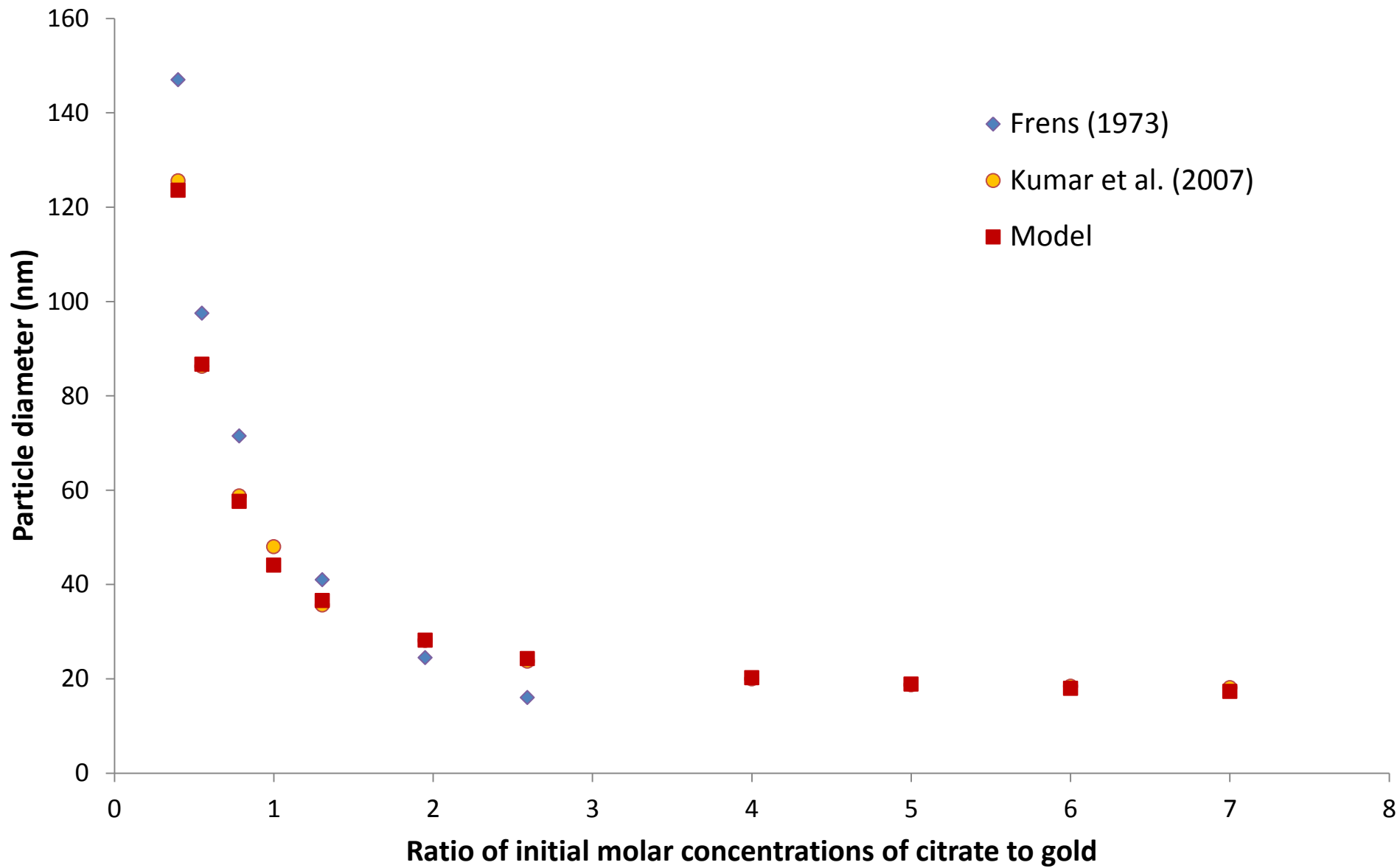
Greek alphabets

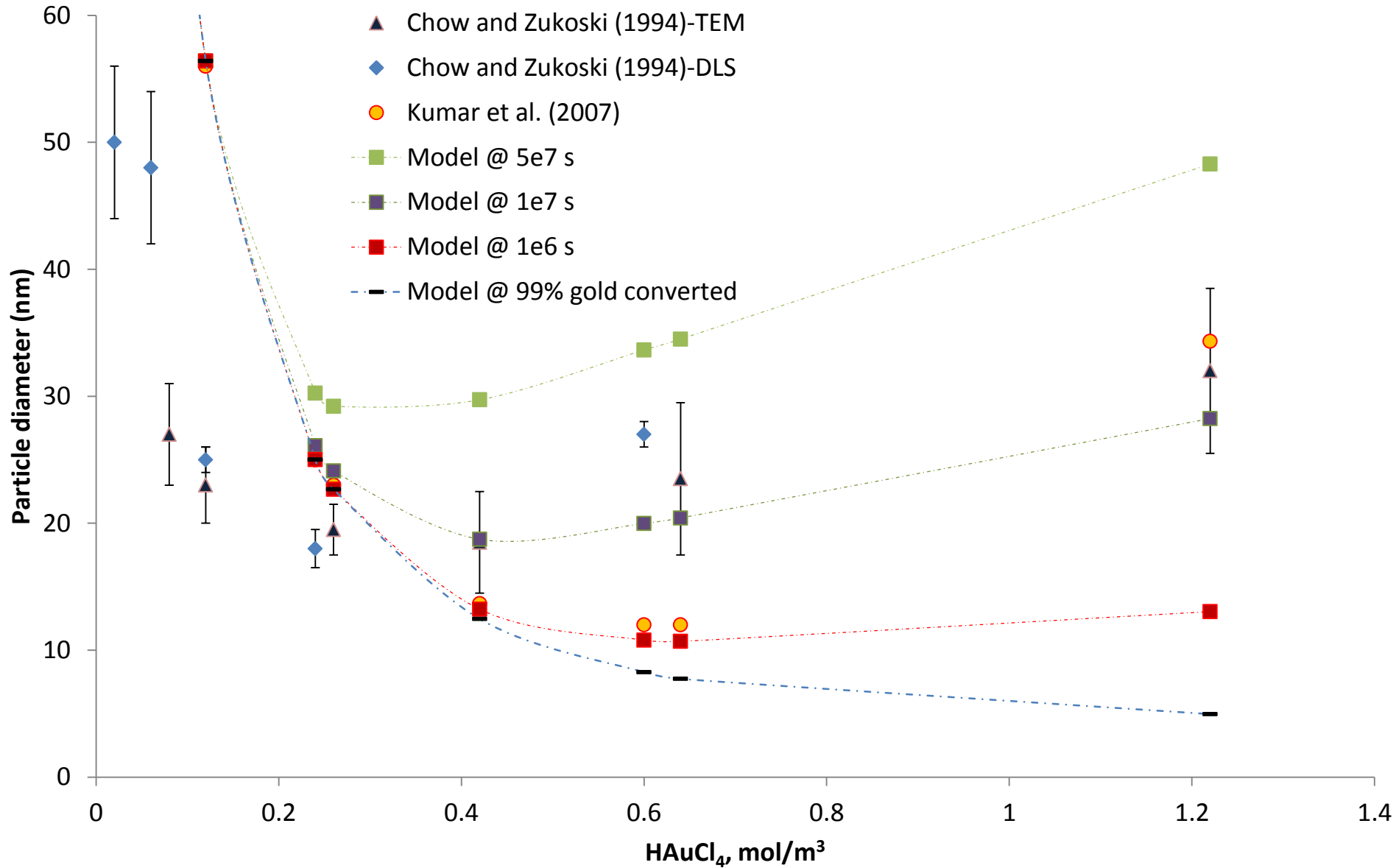
$\alpha(s, s')$	Aggregation kernel	m^3/s
κ	the Debye-Huckel parameter	m
μ	Fluid viscosity	$kg/(m \cdot s)$
ρ	Molar density of gold	mol/m^3
φ	Surface potential	mV
τ	Characteristic time	s

References

1. Kumar, S.; Kumar, R.; Gandhi, K. S. Modeling of Formation of Gold Nanoparticles by Citrate Method. *Ind. Eng. Chem. Res.* **2007**, *46*, 3128-3136
2. Takiyama, K. Formation and Aging of Precipitates. VIII. Formation of Monodisperse Particles (1) Gold Sol Particles by Sodium Citrate Method. *Bull. Chem. Soc. Jpn.* **1958**, *31*, 944–950.
3. Chunfang Li, Dongxiang Li, Ganggiang Wan, Jie Xu and Wanguo Hou, “Facile synthesis of concentrated gold nanoparticles with low size-distribution in water: temperature and pH control”, *Nanoscale Research Letters*, vol. 6, p.440, **2011**
4. K. Zabetakis, W.E. Ghann, S. Kumar, and M.-C. Daniel, *Gold Bull.* *45*, 203 (**2012**).
5. Frens, G. Controlled Nucleation for the Regulation of the Particle Size in Monodisperse Gold Suspensions. *Nature* **1973**, *241*, 20.
6. Turkevich, J.; Stevenson, P.; Hillier, J. A Study of the Nucleation and Growth Process in the Synthesis of Colloidal Gold. *Discuss. Faraday Soc.* **1951**, *11*, 55.
7. Polte, J.; Eiler, R.; Thünemann, A. F.; Sokolov, S.; Ahner, T. T.; Rademann, K.; Emmerling, F.; Kraehnert, R. Nucleation and Growth of Gold Nanoparticles Studied via in situ Small Angle X-ray Scattering at Millisecond Time Resolution. *ACS Nano* **2010**, *4*, 1076–1082.
8. Ji, X. H.; Song, X. N.; Li, J.; Bai, Y. B.; Yang, W. S.; Peng, X. G. *J. Am. Chem. Soc.* **2007**, *129*, 13939.
9. S.K. Sivaraman, S. Kumar, V. Santhanam *Gold Bull.*, *43* (**2010**), pp. 275–285
10. Tamar Dreifuss, Oshra Betzer, Malka Shilo, Aron Popovtzer, Menachem Motieia and Rachela Popovtzer A challenge for theranostics: is the optimal particle for therapy also optimal for diagnostics? *Nanoscale*, **2015**, *7*, 15175.
11. Liveri, V. T., *Controlled Synthesis of Nanoparticles in Microheterogeneous Systems*, *Nanostructure Science and Technology*, Springer Science, **2006**.
12. Chow, M.; Zukoski, C. Gold Sol Formation Mechanisms: Role of Colloidal Stability. *J. Colloid Interface Sci.* **1994**, *165*, 97.

13. M. Wuithschick, S. Witte, F. Kettemann, K. Rademann, J. Polte *Phys. Chem. Chem. Phys.* **2015**, *17*, 19895-19900
14. Abid, J.-P. Laser Induced Synthesis and Nonlinear Optical Properties of Metal Nanoparticles. Ph.D. Thesis, Ecole Polytechnique Federale de Lausanne, Lausanne, Switzerland, **2003**.
15. Freund, P.; Spiro, M. Colloidal Catalysis: The Effect of Sol Size and concentration. *J. Phys. Chem.* **1985**, *89*, 1074.
16. Grosch, R; Briesen, H; Getting Started with Parsival – A Tutorial Introduction; CiT GmbH, **2005**.
17. Mellor J. W. A comprehensive treatise on inorganic and theoretical chemistry. Vol. 3. **1946**. p. 593.
18. Davies, A. The Kinetics of the Coagulation of Gold Sols. *J. Phys. Chem.* **1929**, *33*, 274.
19. Marchisio, D. L. & Fox, R. O. **2013**; Computational Models for Polydisperse Particulate and Multiphase Systems; Cambridge University Press.
20. Ojea-Jiménez, I.; Campanera, J. M. Molecular Modeling of the Reduction mechanism in the Citrate-Mediated Synthesis of Gold Nanoparticles. *J. Phys. Chem. C* **2012**, *116*, 23682–23691.
21. Chunfang Li, Dongxiang Li, Ganggang Wan, Jie Xu and Wanguo Hou, "Facile synthesis of concentrated gold nanoparticles with low size-distribution in water: temperature and pH control", *Nanoscale Research Letters*, vol. 6, p. 440, **2011**.
22. Wei Wang, Ning Li, and Stan Speaker External Factors Affecting Protein Aggregation, Hoboken, NJ, USA: John Wiley & Sons, Inc. **2010**
23. Liveri, V. T., Controlled Synthesis of Nanoparticles in Microheterogeneous Systems, Nanostructure Science and Technology, Springer Science, **2006**.
24. Tamar Dreifuss, Oshra Betzer, Malka Shilo, Aron Popovtzer, Menachem Motieia and Rachela Popovtzer A challenge for theranostics: is the optimal particle for therapy also optimal for diagnostics? *Nanoscale*, **2015**, *7*, 15175.
25. Kettemann, F.; Birnbaum, A.; Witte, S.; Wuithschick, M.; Pinna, N.; Kraehnert, R.; Rademann, K.; Polte, J. *Chem. Mater.* **2016**, *28* (11), 4072-4081.



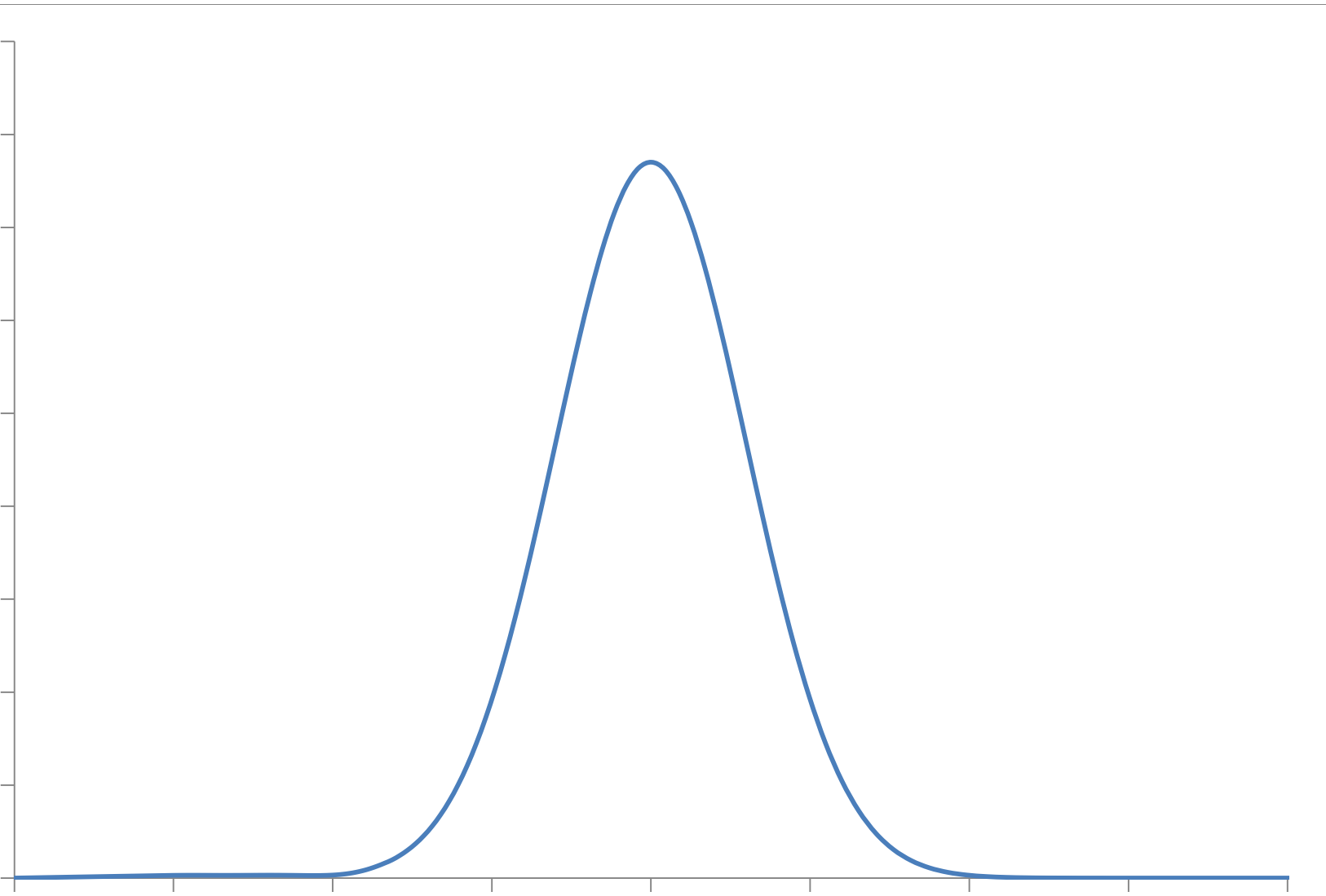


Number density (#/m)

1.8E+11
1.6E+11
1.4E+11
1.2E+11
1E+11
8E+10
6E+10
4E+10
2E+10
0

0.0 0.5 1.0 1.5 2.0 2.5 3.0 3.5 4.0

Particle diameter (nm)

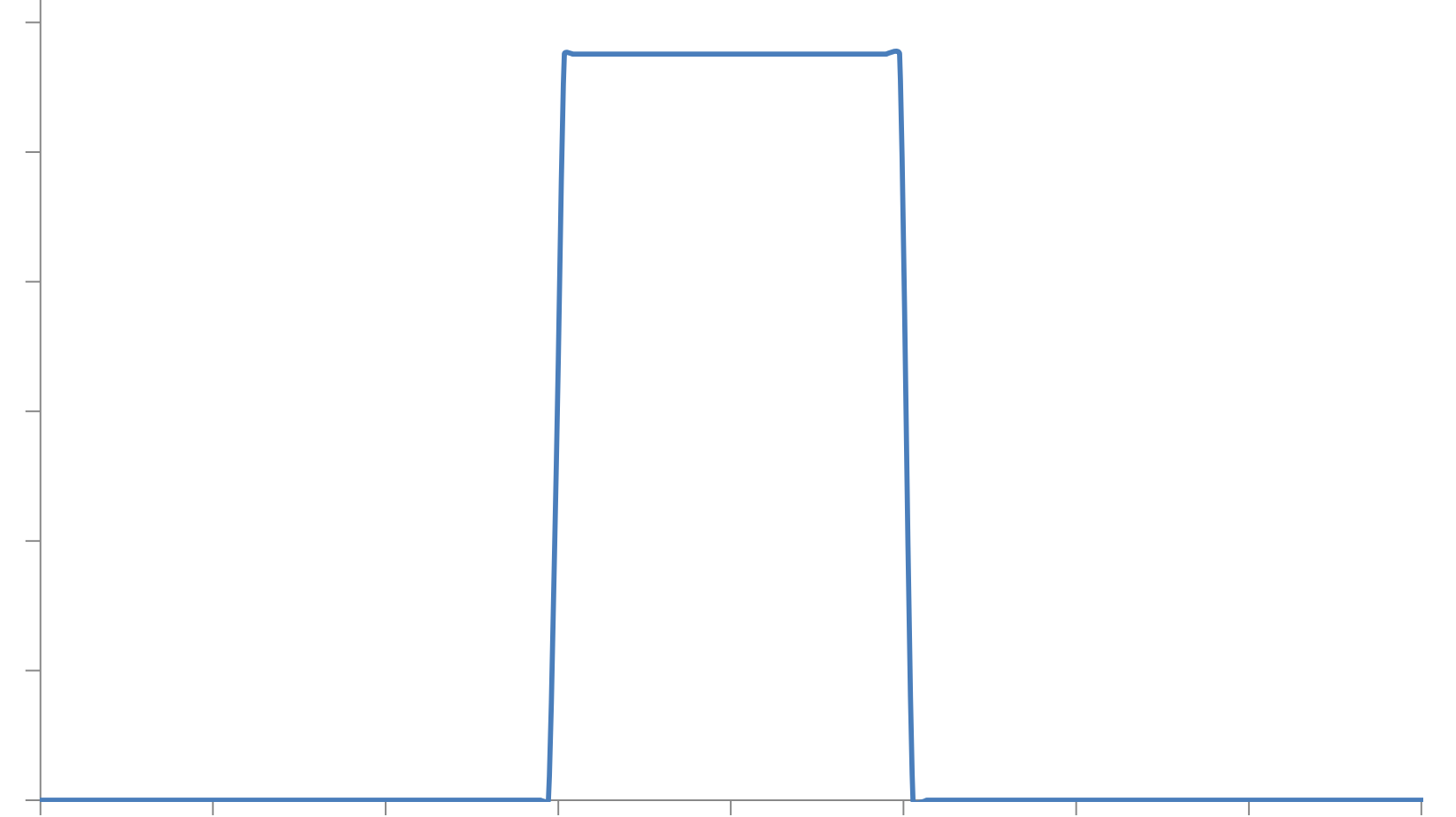


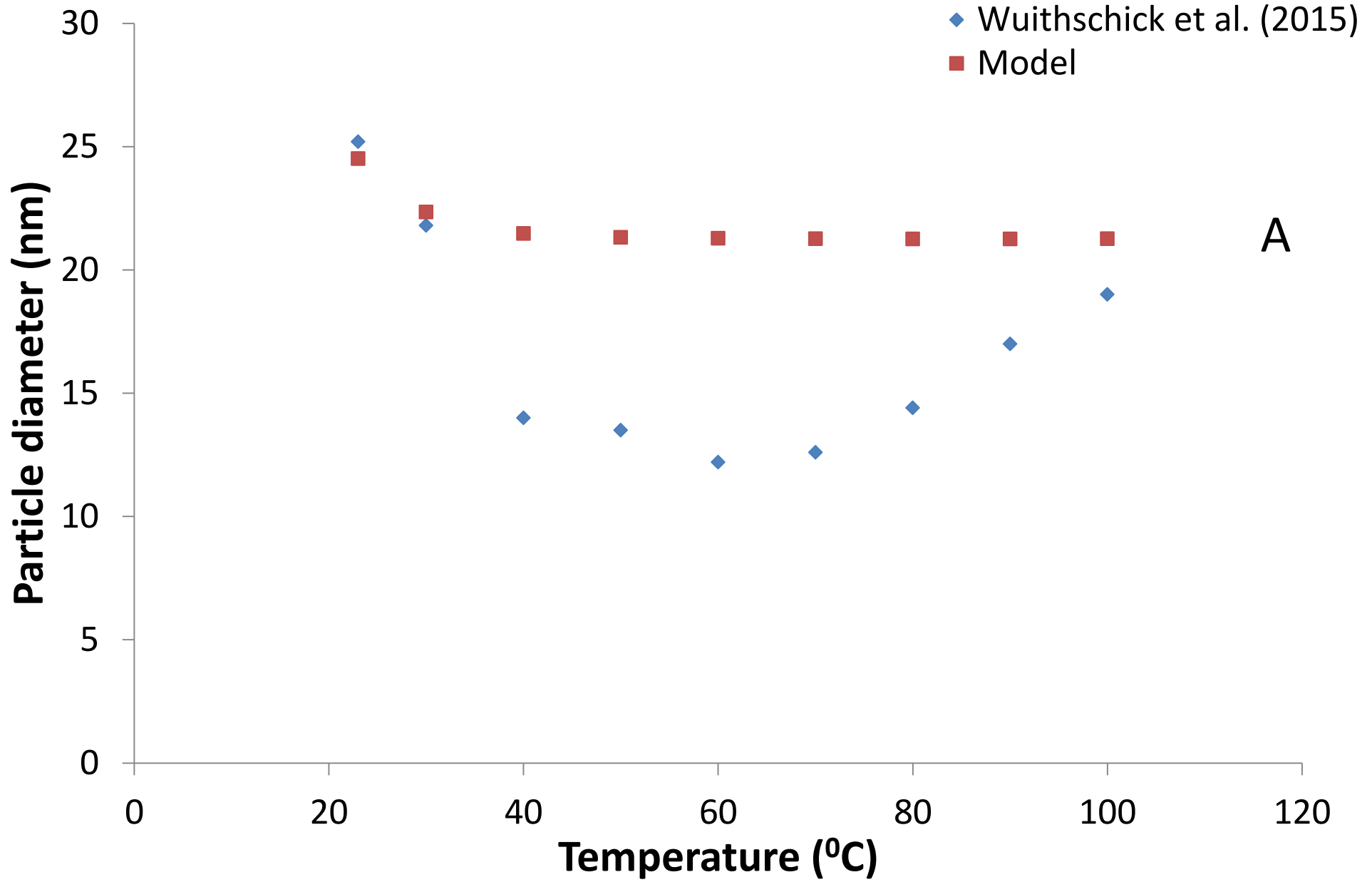
Number density (#/m)

1.4E+11
1.2E+11
1E+11
8E+10
6E+10
4E+10
2E+10
0

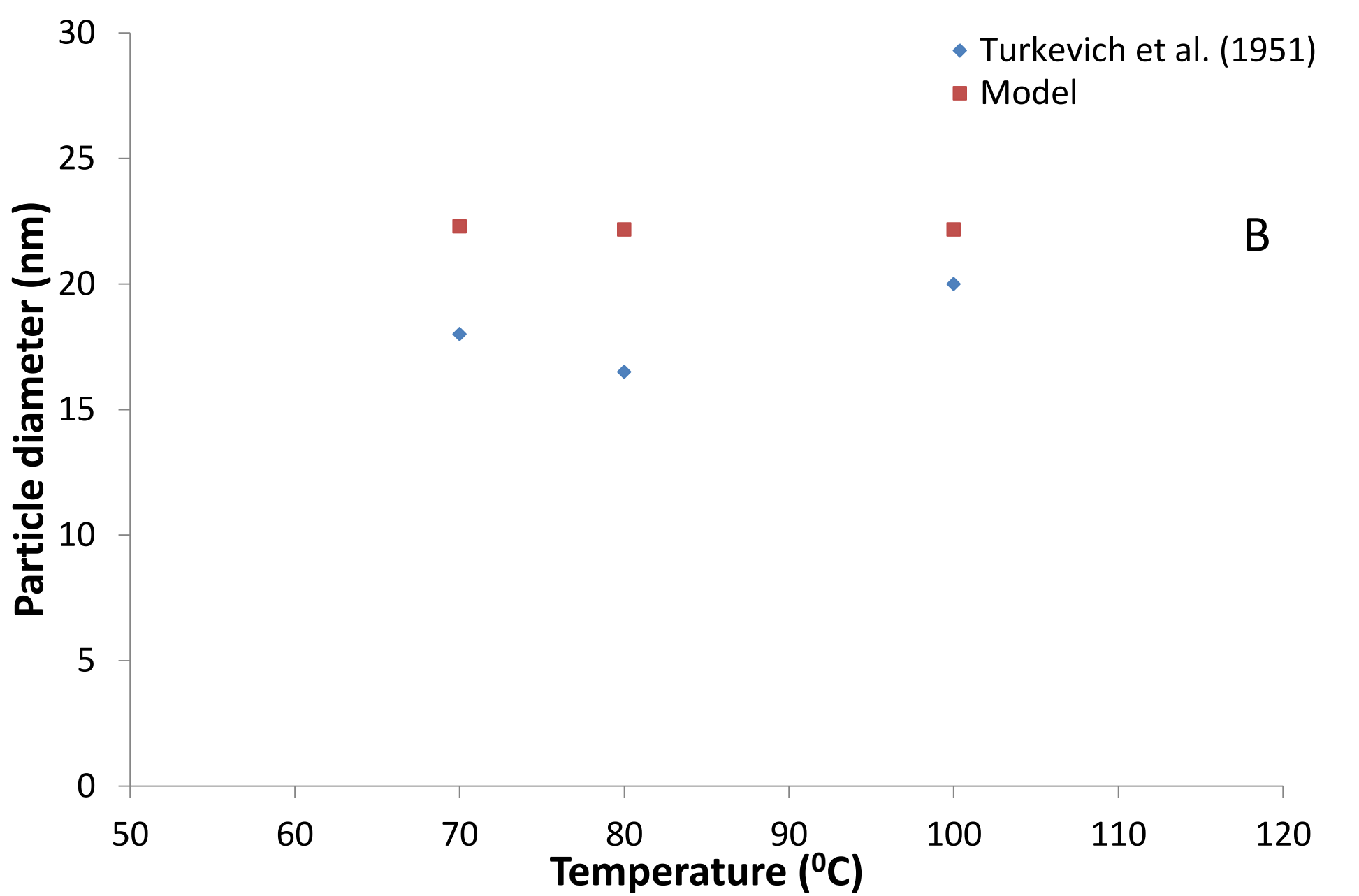
0.0 0.5 1.0 1.5 2.0 2.5 3.0 3.5 4.0

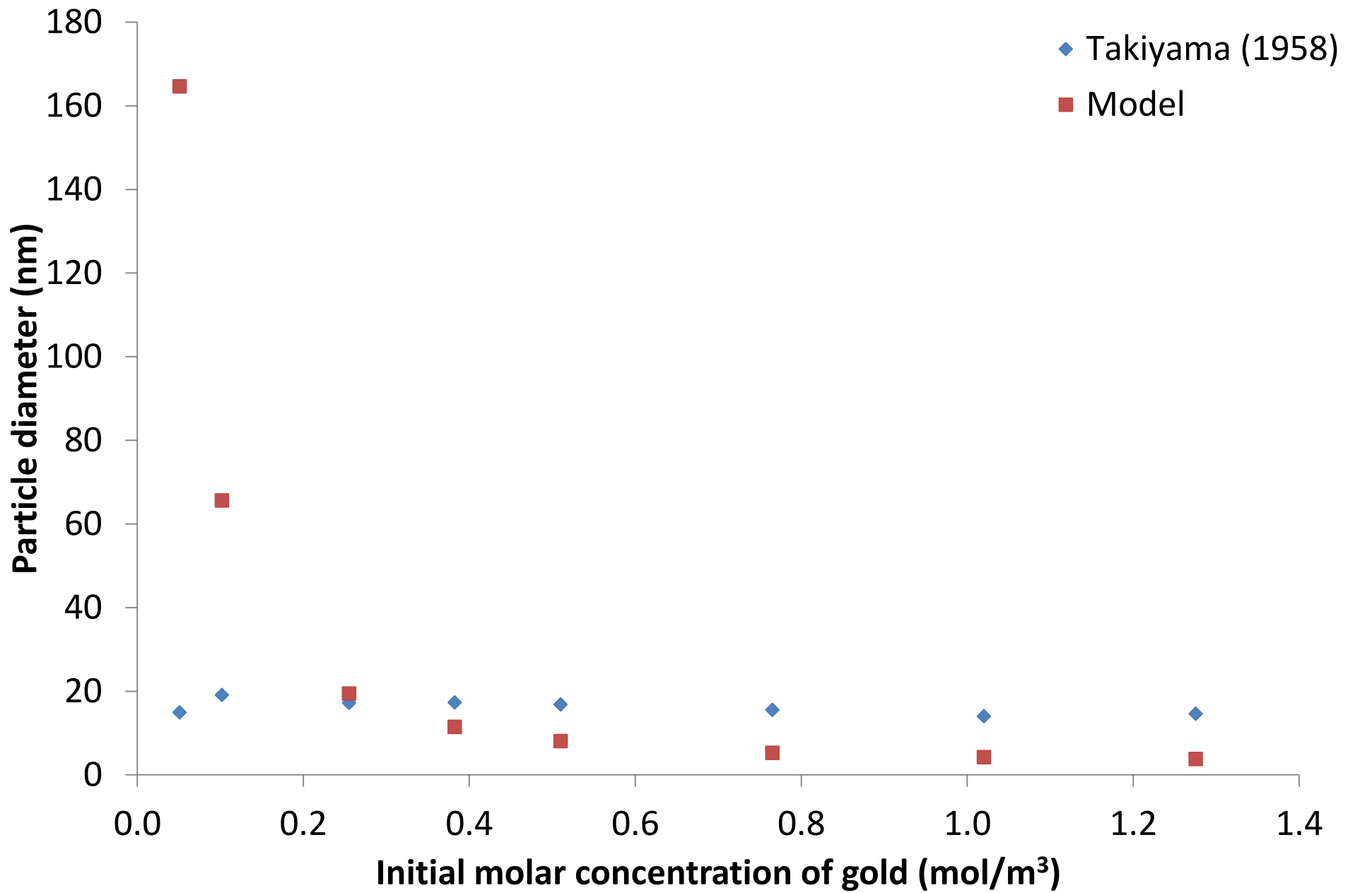
Particle diameter (nm)

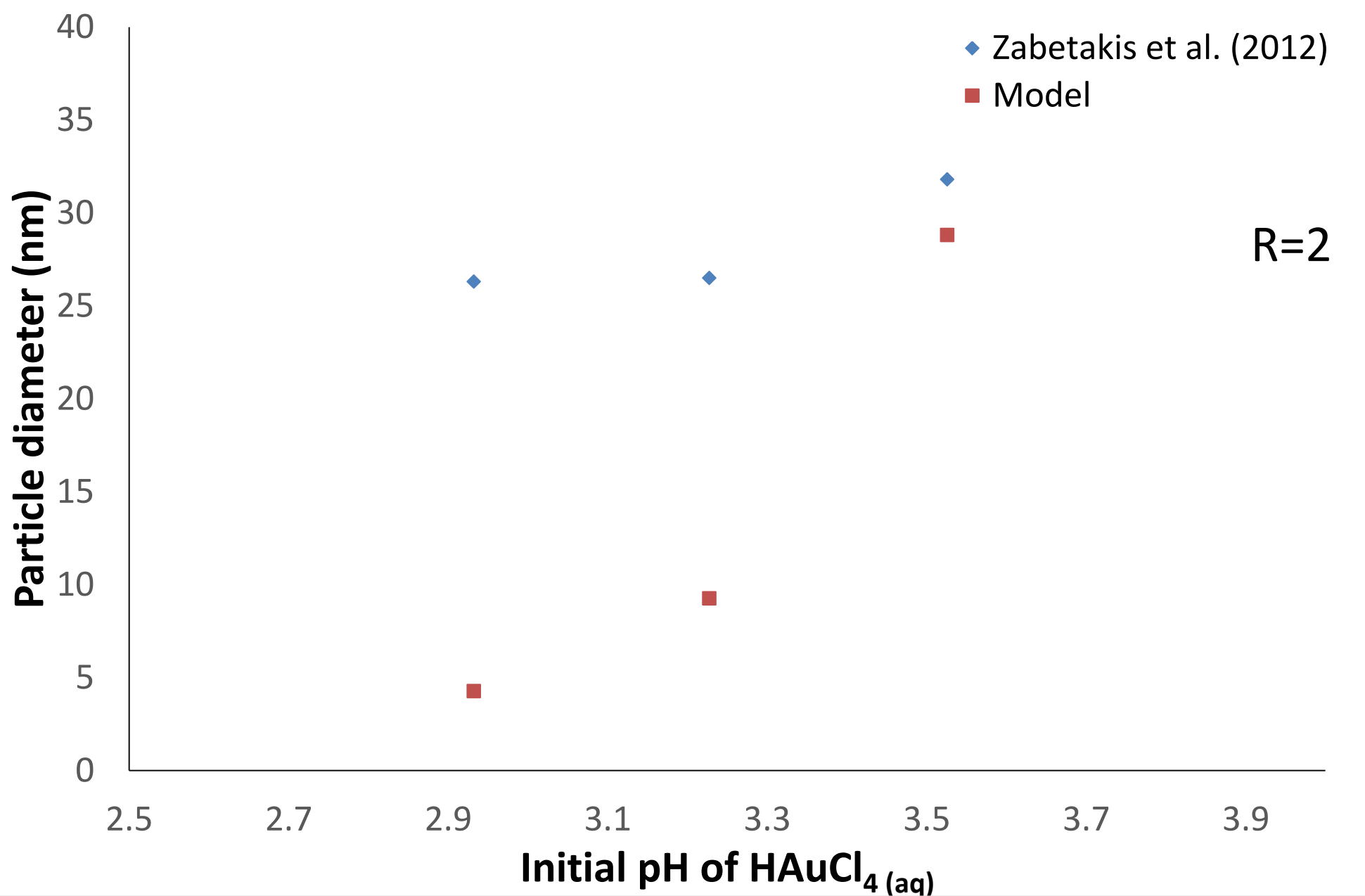


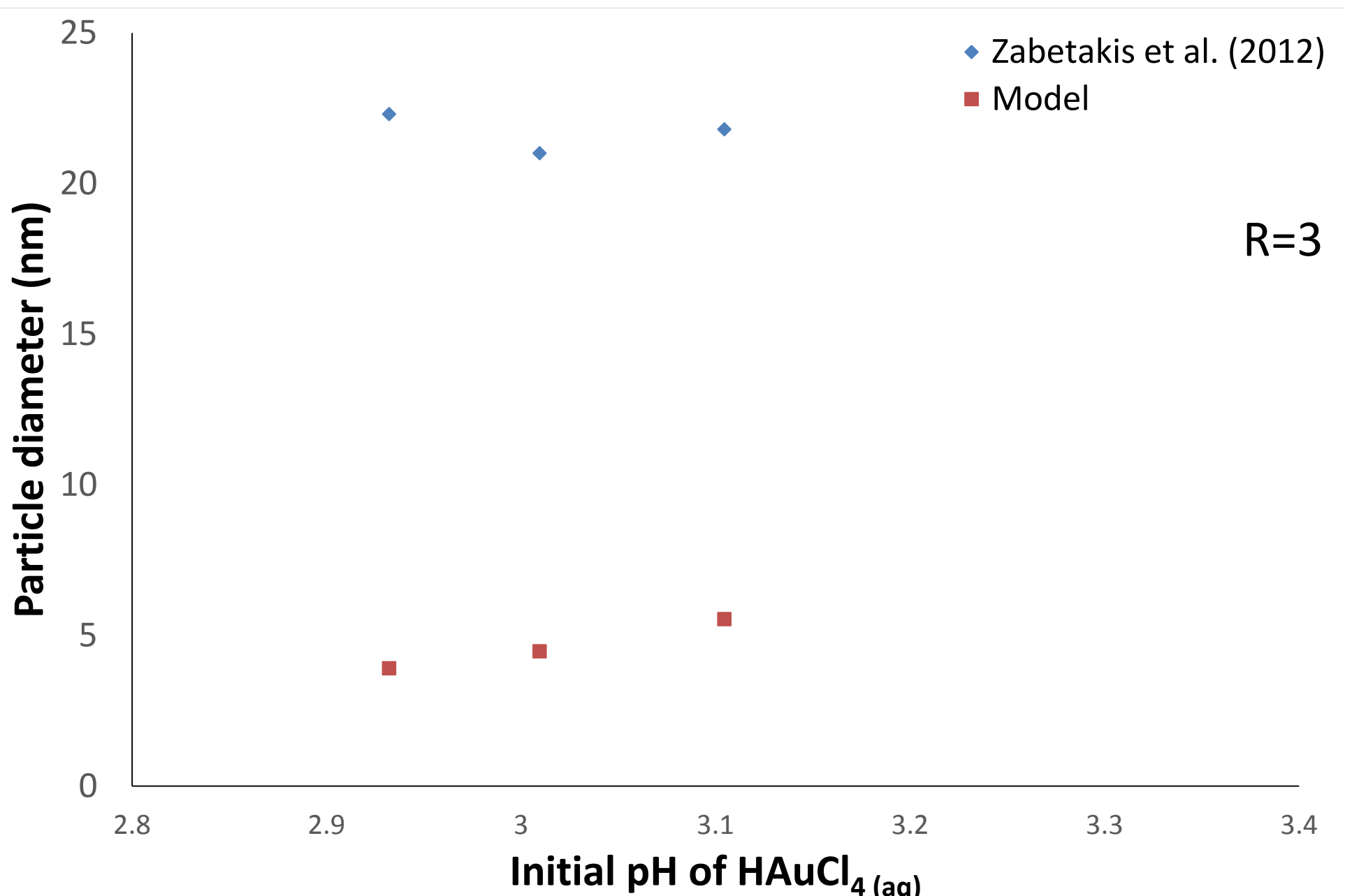


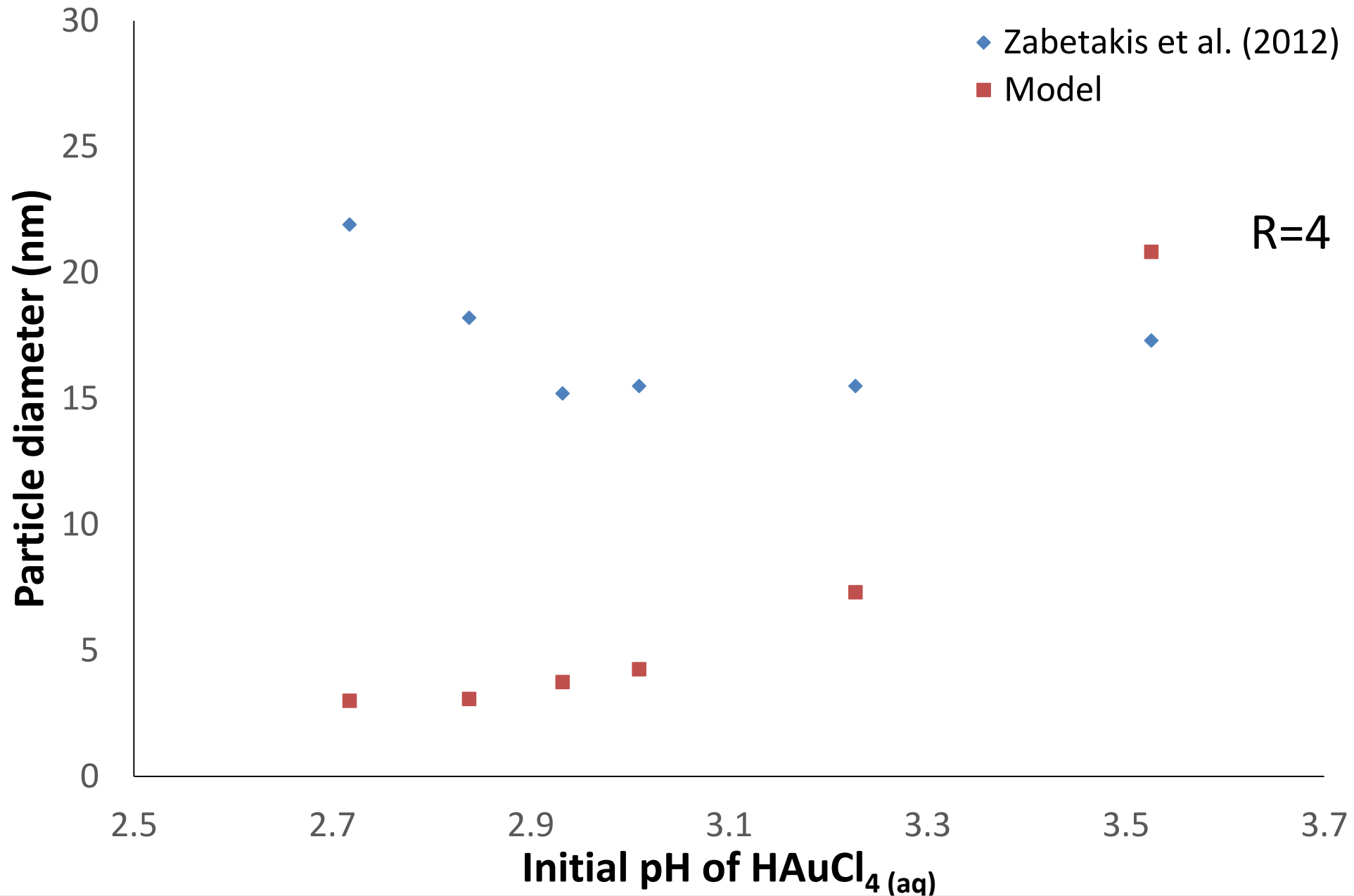
A

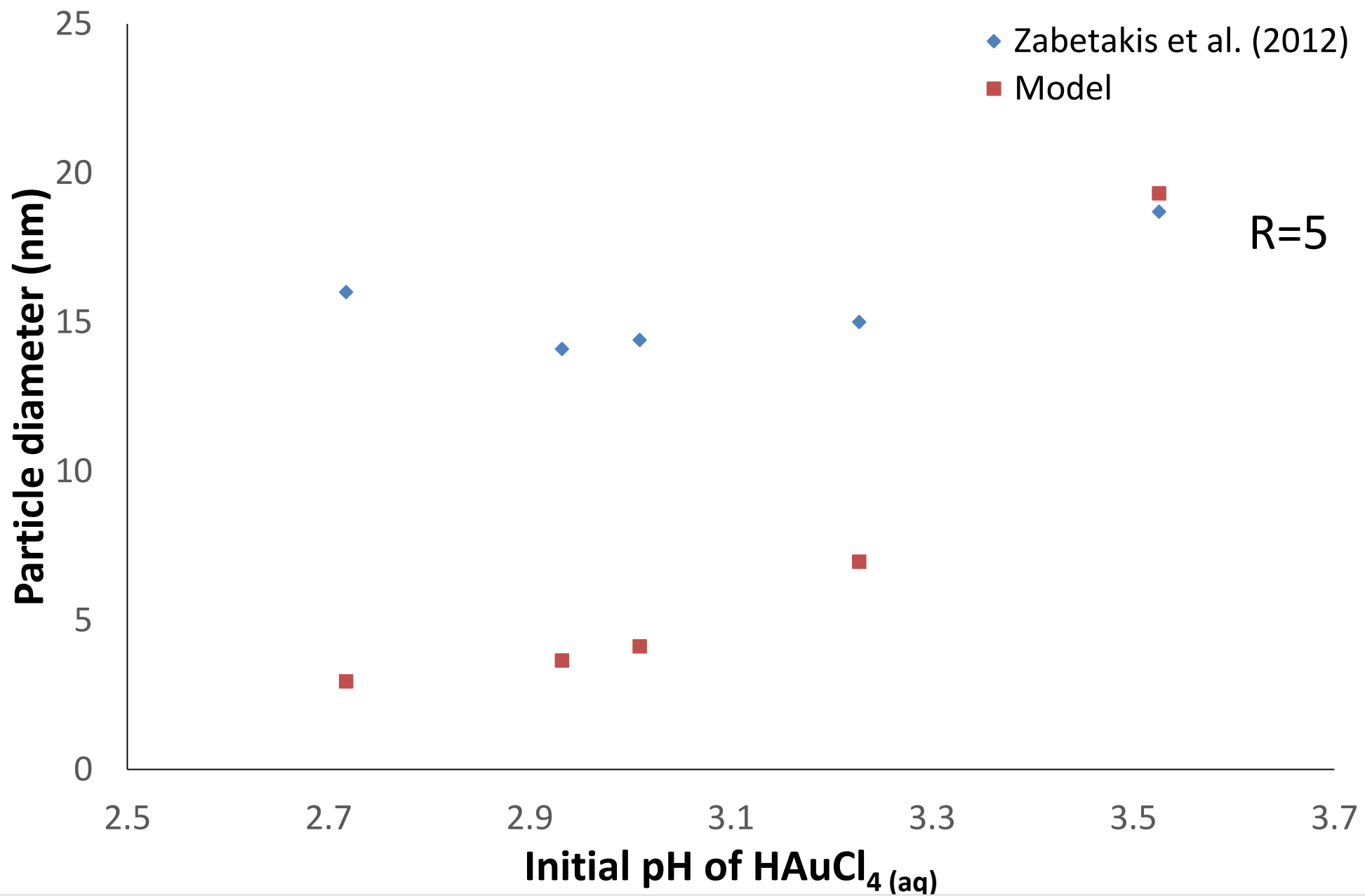


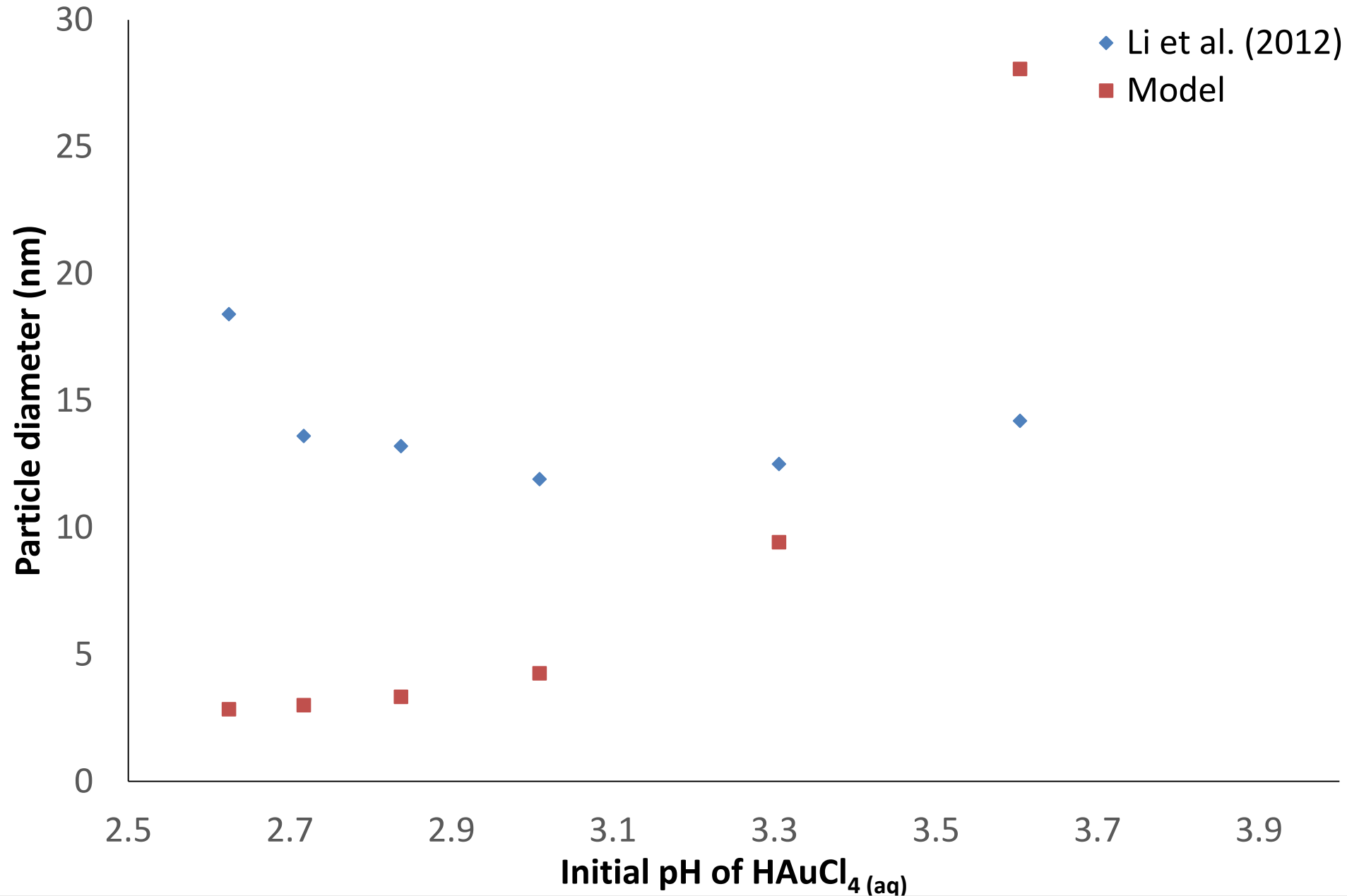












Particle diameter (nm)

◆ Ji et al. (2007)
■ Model

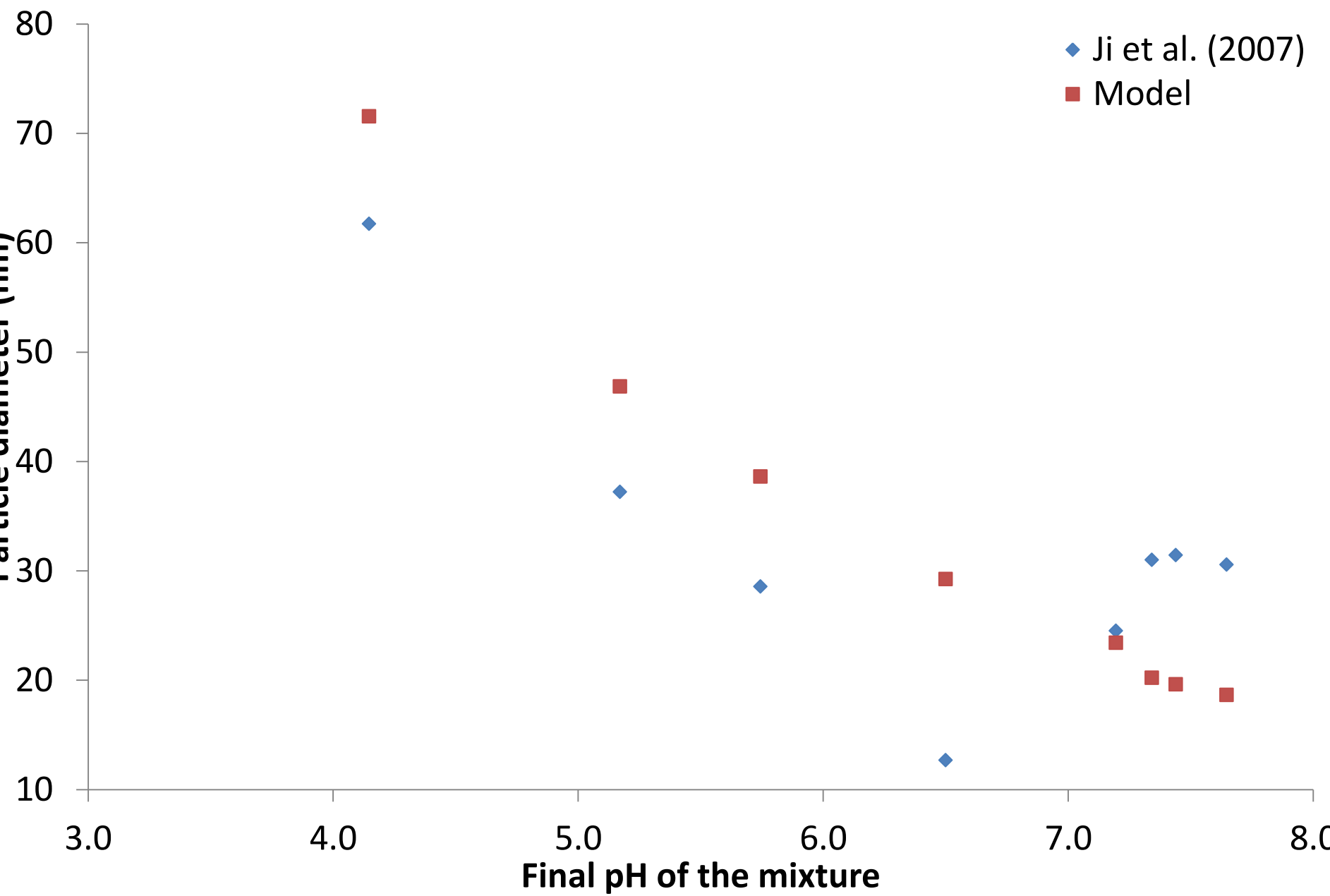


Figure captions

Figure 4.1. Comparison of the predictions of the model implemented in this work for Case 1 with those of the model of Kumar et al. (2007) and with the data of Frens (1973).

Figure 4.2. Comparison of the predictions of the model implemented in this work for Case 2 with those of the model of Kumar et al. (2007) and with the data of Chow and Zukoski (1994). The figure illustrates how aggregation affects the mean particle size at different simulation times.

Figure 4.3. Particle size distributions used to initialize the simulations and for describe the nucleation process in Parsival. Distribution D1 is on the left, while distribution D2 is on the right.

Figure 5.1. Comparison of the model predictions at different temperatures with the data of (A) Wuithschick et al. (2015) and (B) Turkevich et al. (1951).

Figure 5.2. Comparison of the model predictions at different gold concentrations with the data of Takiyama (1958).

Figure 5.3. Comparison of the model predictions at different initial pH with the data of Zabetakis et al. (2012). R represents the ratio of citrate to gold.

Figure 5.4. Comparison of the model predictions at different initial pH with the data of Li et al. (2012).

Figure 5.5. Comparison of the model predictions at different final pH with the data of Ji et al. (2007).

Table 2.1. Summary of the chemical reactions, with their kinetic rate equations and rate constants.

Chemical Reactions	Kinetic rate equations, r	Kinetic rate constants, k
$T + C \xrightarrow{k_c} M + S$	$r_c = -k_c C_T C_C$	$k_c = 1.25 \text{ m}^3/(\text{mol}\cdot\text{s})$
$3M \xrightarrow{k_n, S} \text{nucleus} + T$	$r_{M1} = -3k_n \rho v_0 C_M^3 C_S^2$	$k_n = N_{av} 1.67 \times 10^{-3} (\text{m}^3/\text{mol})^5 1/(\text{m}^3\cdot\text{s})$

$3M \xrightarrow{k_h, \text{particles}} T$ + particle mass	r_{M2} $= -3k_h C_M \int_{v_0}^{\infty} v^{2/3} P(v) dv$	$k_h = 2.5 \times 10^{-4} \text{ m}^3 / (\text{m}^2 \cdot \text{s})$
$S \xrightarrow{k_s} D$	$r_S = -k_s C_S$	$k_s = 1 \text{ s}^{-1}$
$D + 2.5T \xrightarrow{k_d} 2.5M + P$	$r_T = -k_d C_T C_D$	$k_d = 4 \times 10^{-1} \text{ m}^3 / (\text{mol} \cdot \text{s})$

Table 5.1. Values of the rate constants of reactions 2 and 4 with temperature.

Temperature ($^{\circ}\text{C}$)	k_n	k_s	k_n/k_s
23	6.61E+15	6.57E-06	1.01E+21
30	2.51E+16	2.50E-05	1.01E+21
40	1.53E+17	1.52E-04	1.01E+21
50	8.29E+17	8.25E-04	1.01E+21
60	4.07E+18	4.05E-03	1.01E+21
70	1.82E+19	1.81E-02	1.01E+21

80	7.48E+19	7.44E-02	1.01E+21
90	2.84E+20	2.83E-01	1.01E+21
100	1.01E+21	1.00E+00	1.01E+21

ACCEPTED MANUSCRIPT

Highlights

- The mathematical model of Kumar et al. (2007), based on the “Turkevich organizer theory”, was investigated.
- To analyse the model, we tested its predictions against several experimental data reported in the literature.
- The model does not yield satisfactory predictions in various cases, because it is based on a mechanistic description of the particle synthesis that does not account for the acid-base properties of the reactants.
- A novel model, with a more accurate mechanistic description of the synthesis and of the chemistry involved, is required.

Supporting Information

Appendix A

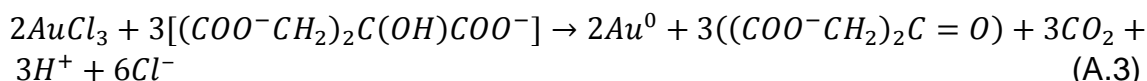
In the article of Kumar et al. (2007), to which we refer the reader, the reduction of auric chloride by acetone is given as:



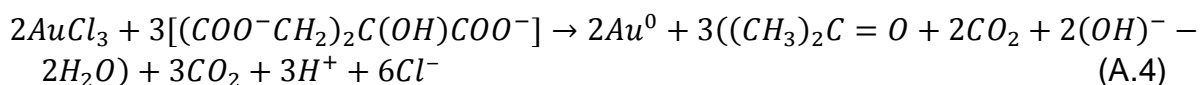
In eq. (A.1), the stoichiometry of acetone to aurous chloride is assumed to be 1: x . To determine x , we substitute for dicarboxy acetone (DCA). The chemical equation for the decomposition of dicarboxy acetone is:



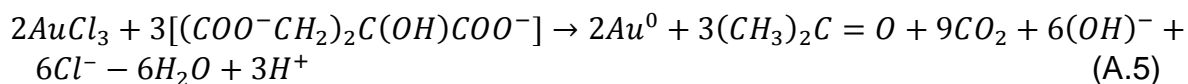
The overall chemical reaction for the Turkevich synthesis to produce gold atoms in excess of citrate is:



By introducing eq. (A.2) in eq. (A.3), we have:



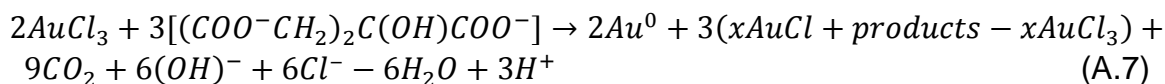
Expanding eq. (A.4) yields:



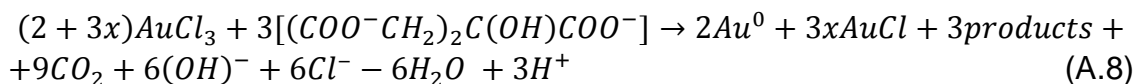
We now write eq. (A.1) as follows:



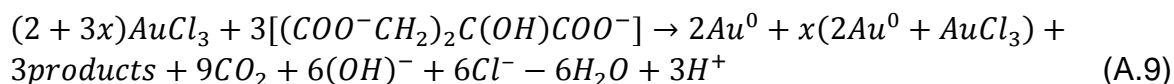
and then introduce it into eq. (A.5) to eliminate acetone; this yields:



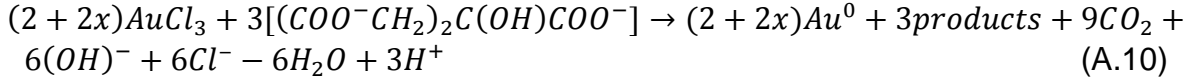
We now rearrange eq. (A.7) as follows:



Using the reaction $3AuCl \rightarrow 2Au^0 + AuCl_3$ in eq. (A.8), we obtain:



or equivalently:



This is the final overall reaction, from which we can calculate the value of x using $citrate/gold = \sim 0.43$. The result is $x = 2.49$, which differs from the value 4 reported in Kumar et al. (2007).

Appendix B

Parsival is a simulation program for solving population balance equations (PBEs). The form of the PBE that Parsival solves is reported in eq. (B.1), where it is assumed that the system is closed and uniform (that is, perfectly mixed).

$$\partial_t f(s) = -\partial_s[G_s(s)f(s)] + J_{nuc}(s) + B(s) - D(s) \quad (B.1)$$

where the meaning of the symbols is given in the main manuscript; in particular, $f(s)$ represents the number of particles per unit volume of physical and particle-diameter space (so, it is a number density in a four-dimensional phase space) at time t .

The equation reveals that in Parsival the variable characterizing the internal state of the particles (the so-called internal variable) is the particle diameter s ; in the original model of Kumar et al. (2007), on the other hand, the internal variable is the particle volume v . Thus, the PBE solved in the original model is:

$$\partial_t P(v) = -\partial_v[G_v(v)P(v)] + J_{nuc}(v) + B(v) - D(v) \quad (B.2)$$

where the meaning of the symbols is given in the main manuscript; in particular, $P(v)$ represents the number of particles per unit volume of physical and particle-volume space. Moreover, it is:

$$J_{nuc}(v) = 2k_n C_M^3 C_S^2 \delta(v - v_0) \quad (B.3)$$

$$G_v(v) = 2 \frac{k_h}{\rho} C_M v^{2/3} \quad (B.4)$$

$$B(v) - D(v) = \frac{1}{2} \int_{v_0}^v \frac{q(v-v',v')}{W} P(v-v') P(v') dv' - P(v) \int_{v_0}^{\infty} \frac{q(v,v')}{W} P(v') dv' \quad (B.5)$$

$$q(v, v') = \frac{2K_B T}{3\mu} \left(\frac{1}{v^{1/3}} + \frac{1}{v'^{1/3}} \right) (v^{1/3} + v'^{1/3}) \quad (B.6)$$

To obtain eq. (B.1) from eq. (B.2), a variable transformation, which we report below, is thus necessary. We start by writing:

$$v \equiv m_v s^3 \quad (B.7)$$

where v and s , as said, are the particle volume and diameter, respectively, while m_v is the volume shape factor. Thus, we can write:

$$dv = 3m_v s^2 ds \quad (B.8)$$

Next, by definition, it is:

$$P(v) dv \equiv f(s) ds \quad (B.9)$$

If we use eq. (B.8), the equation above yields:

$$P(v) = \left(\frac{1}{3m_v s^2} \right) f(s) \quad (\text{B.10})$$

Similarly, one can show that:

$$\partial_t P(v) = \left(\frac{1}{3m_v s^2} \right) \partial_t f(s) \quad (\text{B.11})$$

$$2k_n C_M^3 C_S^2 \delta(v - v_0) = \left(\frac{1}{3m_v s^2} \right) 2k_n C_M^3 C_S^2 \delta(s - s_0) \quad (\text{B.12})$$

$$2 \frac{k_h}{\rho} C_M \partial_v [v^{2/3} P(v)] = \left(\frac{1}{9m_v^{4/3} s^2} \right) 2 \frac{k_h}{\rho} C_M \partial_s f(s) \quad (\text{B.13})$$

$$\int_{v_0}^{\infty} v^{2/3} P(v) dv = m_v \int_{s_0}^{\infty} s^2 f(s, t) ds \quad (\text{B.14})$$

For the aggregation submodel, we first substitute eq. (B.7) for v in eq. (B.6); doing so yields:

$$q(v, v') = \alpha(s, s') = \frac{2k_B T}{3\mu} \left(\frac{1}{s} + \frac{1}{s'} \right) (s + s') \quad (\text{B.15})$$

Similarly, it is:

$$q(v - v', v') = \alpha(\xi, s') = \frac{2k_B T}{3\mu} \left(\frac{1}{\xi} + \frac{1}{s'} \right) (\xi + s') \quad (\text{B.16})$$

where:

$$v - v' = m_v \xi^3 \quad \text{and} \quad \xi^3 \equiv s^3 - s'^3 \quad (\text{B.17})$$

This relation, along with the following:

$$P(v') = \left(\frac{1}{3m_v s'^2} \right) f(s') \quad ; \quad P(v - v') = \left(\frac{1}{3m_v \xi^2} \right) f(\xi) \quad ; \quad dv' = 3m_v s'^2 ds' \quad (\text{B.18})$$

allow us to write:

$$\frac{1}{2} \int_{v_0}^v \frac{q(v-v', v')}{W} P(v - v') P(v') dv' = \frac{1}{2} \int_{s_0}^s \frac{\alpha(\xi, s')}{W} \frac{f(\xi) f(s')}{3m_v \xi^2} ds' \quad (\text{B.19})$$

and:

$$P(v) \int_{v_0}^{\infty} \frac{q(v, v')}{W} P(v') dv' = \frac{f(s)}{3m_v s^2} \int_{s_0}^{\infty} \frac{\alpha(s, s')}{W} f(s') ds' \quad (\text{B.20})$$

Using all the equations derived above, we finally obtain:

$$J_{nuc}(s) = 2k_n C_M^3 C_S^2 \delta(s - s_0) \quad (\text{B.21})$$

$$G_S(s) = \frac{2}{3} \frac{k_h}{m_v^{1/3}} \frac{C_M}{\rho} \quad (\text{B.22})$$

$$B(s) - D(s) = \frac{1}{2} \int_{s_0}^s \frac{\alpha(\xi, s')}{W} \frac{s^2}{\xi^2} f(s', t) f(\xi, t) ds' - f(s, t) \int_{s_0}^{\infty} \frac{\alpha(s, s')}{W} f(s', t) ds' \quad (\text{B.23})$$

which, substituted in eq. (B.1), yields the form of the PBE that we solved in Parsival.

Appendix C

We estimate the characteristic time for the first four reactions involved in the GNPs synthesis to see how the reactions progress relative to each other. The characteristic time of a reaction indicates how long the reaction requires to convert a “significant” amount of the limiting reactant.

Reaction 1

Assuming that $C_{T_0} = C_{C_0} = 0.3 \text{ mol/m}^3$, and given the stoichiometry of the reaction, we can write:

$$\frac{dC_T}{dt} = -k_c C_T C_C = -k_c C_T^2 \quad (\text{C.1})$$

The characteristic time is therefore equal to:

$$\tau_c \sim \frac{1}{k_c C_{T_0}} = \frac{1}{1.25 \times 0.3} \text{ s} \sim 1 \text{ s}$$

Since this is a second-order reaction, the time that the reaction takes to reduce the concentration of component T to 10% of its original value is ca. $10 \tau_c$. Over a time τ_c the reagent concentration reduces to about 50% of its original value.

Reaction 2

$$\frac{dC_M}{dt} = -(3k_n \rho v_0 C_S^2) C_M^3 \quad (\text{C.2})$$

$C_{M_{max}} = C_{S_{max}} = 0.3 \text{ mol/m}^3$ are the maximum concentration values for M and S , if we assume that reaction 1 is complete. Assuming that S does not react (in this reaction it behaves as a catalyst, and, for the time being, we do not consider reaction 4, which consumes S), in the equation above the variable C_S can be replaced with the constant $C_{S_{max}}$. Thus, the reaction is third-order and we can write:

$$\begin{aligned} \tau_n &\sim \frac{1}{(3k_n \rho v_0 C_{S_{max}}^2) C_{M_{max}}^2} \\ &= \frac{1}{3 \times 1.0053 \cdot 10^{21} \times 10^5 \times 4.18 \cdot 10^{-27} \times 0.3^4} \text{ s} = 98.72 \text{ s} \sim 100 \text{ s} \end{aligned}$$

Because this is a third-order reaction, the time that the reaction takes to reduce the concentration of component M to 10% of its original value is ca. $50 \tau_n$. Over a time τ_n the reagent concentration reduces to about 58% of its original value.

The values reported above hold in the assumption that C_S is constant. But reaction 4 depletes component S, reducing its concentration significantly in about one second (see below). Accordingly, over this time interval, C_S decreases, making τ_n increase rapidly. So, in the end, reaction 2 proceeds for a very short time.

Reaction 3

We take the nuclei number density to be equal to 10^{17} 1/m^3 (refer to Appendix D). Assuming that nucleation and growth are fully decoupled and that, once nucleation is over, no aggregation takes place, the particle number density can be taken equal to 10^{17} 1/m^3 . So, we can estimate the order of magnitude of the particle surface per unit volume of physical space as follows:

$$\int_{v_0}^{\infty} v^{2/3} P(v) dv \sim (4.18 \times 10^{-27})^{2/3} \times 10^{17} = 0.26 \text{ m}^2/\text{m}^3$$

We can then write:

$$\frac{dC_M}{dt} = - (3k_h \int_{v_0}^{\infty} v^{2/3} P(v) dv) C_M \quad (\text{C.3})$$

Therefore, the reaction is first-order and the characteristic time is:

$$\tau_{h1} \sim \frac{1}{3k_h \int_{v_0}^{\infty} v^{2/3} P(v) dv} = \frac{1}{3 \times 2.50 \cdot 10^{-4} \times 0.26} \text{ s} \sim 5000 \text{ s}$$

In the above, we assumed the total surface area as that of the nuclei. However, with time, this total surface area increases and would reduce τ_{h1} . If we calculate the time scale based on the final particle size, which is 37.5 nm for $C_{T_0} = C_{C_0} = 0.3 \text{ mol/m}^3$, we have:

$$\int_{v_0}^{\infty} v^{2/3} P(v) dv \sim (2.76 \times 10^{-23})^{2/3} \times 10^{17} = 91.35 \text{ m}^2/\text{m}^3$$

and consequently:

$$\tau_{h2} \sim \frac{1}{3k_h \int_{v_0}^{\infty} v^{2/3} P(v) dv} = \frac{1}{3 \times 2.50 \cdot 10^{-4} \times 91.35} \text{ s} \sim 15 \text{ s}$$

Thus, the growth process starts slowly with a time constant of about 5000 s and ends rapidly with a time constant of about 15 s. Therefore, relying also on the results of the numerical simulations, we took the effective growth time constant τ_h to be $\sim 10^2 \text{ s}$, which is an intermediate value between the two estimated above.

The time scale estimated yields the order of magnitude of the time required for 99% conversion of gold into GNPs when $C_{T_0} = C_{C_0} = 0.3 \text{ mol/m}^3$.

Reaction 4

This is a first-order reaction, and so:

$$\tau_s \sim \frac{1}{k_s} = \frac{1}{1.00} \text{ s} \sim 1 \text{ s} \quad (\text{C.4})$$

A significant amount of S therefore degrades in about one second, stopping reaction 2 prematurely.

Appendix D

NPs are most likely to aggregate when their concentration is the highest. To estimate the characteristic time of the aggregation process, we consider the scenario where the aggregation rate is at its maximum value.

According to Marchisio & Fox (2013), the aggregation characteristic time is given by:

$$\tau_a \sim \frac{W}{q(v_s, v_s)N_c} \quad (D.1)$$

Here N_c is the characteristic number concentration of NPs in the system and v_s is the characteristic volume of the NPs. We will consider the minimum value of W , because this favours aggregation. From eqs. (2.10) and (2.11), the minimum value is obtained when $f = 1$, which gives $\varphi = -90 \text{ mV}$. Therefore, it is:

$$\begin{aligned} \ln W &= -\frac{560}{90} \log_{10}[(3C_{C_0} + C_{T_0}) \times 10] + 27.5 \\ &= -\frac{560}{90} \log_{10}[(0.9 + 0.3) \times 10] + 27.5 \quad ; \quad W = 1.06 \times 10^9 \end{aligned}$$

At the conditions at which the synthesis is conducted, $T = 373 \text{ K}$, $\rho = 10^5 \text{ mol/m}^3$ and $\mu = 2.74 \times 10^{-4} \text{ kg/(m.s)}$. Since $K_B = 1.38 \times 10^{-23} \text{ J/K}$, eq. (2.9) gives:

$$q(v_s, v_s) = \frac{2K_B T}{3\mu} \left(\frac{1}{v_s^{1/3}} + \frac{1}{v_s^{1/3}} \right) (v_s^{1/3} + v_s^{1/3}) = \frac{8K_B T}{3\mu} = 5 \times 10^{-17} \text{ m}^3/\text{s}$$

The number of NPs per unit volume of physical space that would form before aggregation starts taking place if reaction 2 went to completion is equal to:

$$N_{c,max} = \frac{2 C_{T_0}}{3 \rho v_0} \quad (D.3)$$

As seen above, to complete, reaction 2 requires $50 \tau_n$ (i.e. 5000 s). But reaction 4 will permit reaction 2 to proceed only for about one second; therefore, it is:

$$N_c \sim \frac{2 C_{T_0}}{3 \times 5000 \rho v_0} = 9.4 \times 10^{16} \text{ 1/m}^3 \quad (D.3)$$

Replacing these results in eq. (D.1), we obtain:

$$\tau_a \sim \frac{1.06 \times 10^9}{5 \times 10^{-17} \times 9.4 \times 10^{16}} = 2.26 \times 10^8 \text{ s} \sim 10^8 \text{ s}$$

This is the characteristic time of the aggregation process for the initial conditions used in the synthesis. It gives an estimate of the time required by the aggregation process to occur significantly.